Developmental Biology 408 (2015) 328–344

Contents lists available at ScienceDirect

Developmental Biology

journal homepage: www.elsevier.com/locate/developmentalbiology

Xenopus pax6 mutants affect eye development and other organ systems, and have phenotypic similarities to human aniridia patients

Takuya Nakayama [a], Marilyn Fisher [a,1], Keisuke Nakajima [b,1], Akinleye O. Odeleye [a,1], Keith B. Zimmerman [a], Margaret B. Fish [a,2], Yoshio Yaoita [b], Jena L. Chojnowski [c], James D. Lauderdale [c], Peter A. Netland [d], Robert M. Grainger [a,d,*]

[a] Department of Biology, University of Virginia, Charlottesville, VA 22904, USA
[b] Division of Embryology and Genetics, Institute for Amphibian Biology, Hiroshima University, Higashihiroshima 739-8526, Japan
[c] Department of Cellular Biology, University of Georgia, Athens, GA, 30602, USA
[d] Department of Ophthalmology, University of Virginia School of Medicine, Charlottesville, VA 22908, USA

ARTICLE INFO

Article history:
Received 28 November 2014
Received in revised form
13 February 2015
Accepted 16 February 2015
Available online 25 February 2015

Keywords:
Xenopus tropicalis
Transcription Activator-Like Effector Nuclease (TALEN)
Lens
Retina
Neural patterning

ABSTRACT

Mutations in the *Pax6* gene cause ocular defects in both vertebrate and invertebrate animal species, and the disease aniridia in humans. Despite extensive experimentation on this gene in multiple species, including humans, we still do not understand the earliest effects on development mediated by this gene. This prompted us to develop *pax6* mutant lines in *Xenopus tropicalis* taking advantage of the utility of the *Xenopus* system for examining early development and in addition to establish a model for studying the human disease aniridia in an accessible lower vertebrate. We have generated mutants in *pax6* by using Transcription Activator-Like Effector Nuclease (TALEN) constructs for gene editing in *X. tropicalis*. Embryos with putative null mutations show severe eye abnormalities and changes in brain development, as assessed by changes in morphology and gene expression. One gene that we found is downregulated very early in development in these *pax6* mutants is *myc*, a gene involved in pluripotency and progenitor cell maintenance and likely a mediator of some key *pax6* functions in the embryo. Changes in gene expression in the developing brain and pancreas reflect other important functions of *pax6* during development. In mutations with partial loss of *pax6* function eye development is initially relatively normal but froglets show an underdeveloped iris, similar to the classic phenotype (aniridia) seen in human patients with *PAX6* mutations. Other eye abnormalities observed in these froglets, including cataracts and corneal defects, are also common in human aniridia. The frog model thus allows us to examine the earliest deficits in eye formation as a result of *pax6* lesions, and provides a useful model for understanding the developmental basis for the aniridia phenotype seen in humans.

Introduction

The transcription factor Pax6 plays an essential role in a highly conserved network of genes controlling eye development in both invertebrates and vertebrates (Callaerts et al., 1997; Gehring and Ikeo, 1999). *Pax6* also plays critical roles outside of the eye, in brain and spinal cord development (Manuel and Price, 2005; Stoykova et al., 1996) as well as in development of the pancreas and intestinal enteroendocrine cells (Hill et al., 1999; St-Onge et al., 1997) and is active throughout development in different phases of organogenesis and into adult life (Osumi et al., 2008). Homozgyous mutations in animals ranging from *Drosophila* (Sturtevant, 1951) to mammals (Hogan et al., 1986; Roberts, 1967) result in eyelessness and phenotypes in other sites of activity as well. In humans heterozygotes develop the syndrome aniridia, so named because patients have no iris (or a poorly formed iris), though the defect is far more pervasive in the eye, leading to defects in the cornea, lens and retina that can result in severe visual deficits that typically increase with age (Hingorani et al., 2012). In this study we use gene-editing tools to generate mutations in the amphibian *Xenopus tropicalis* to study the role of *pax6* both in development and disease.

Study of the function of *pax6* in the amphibian *X. tropicalis* offers the prospect of clarifying its activity at key early stages. In addition, as a diploid *Xenopus* species it is well suited to genetic studies to examine function, and also provides the many overall advantages of the *Xenopus* system (e.g. ready access to large numbers of embryos, suitability for surgical manipulations) for

* Corresponding author at: Department of Biology, University of Virginia, Charlottesville, VA 22904, USA. Fax: +1 434 982 5626.
E-mail address: rmg9p@virginia.edu (R.M. Grainger).
[1] These authors contributed equally to this work.
[2] Present address: Department of Developmental and Cell Biology, University of California, Irvine, CA 92697, USA.

http://dx.doi.org/10.1016/j.ydbio.2015.02.012
0012-1606/

examining early developmental phenomena (Harland and Grainger, 2011).

Mutations in *Pax6* have been discovered or induced in a number of model organisms, providing insight into the function of this gene from a number of perspectives. The *Small eye* (*Sey*) mutant in the mouse is semi-dominant, resulting in heterozygotes with eye deficits (Hogan et al., 1988, 1986), including an aniridia-like phenotype similar to that seen in humans, though in the mouse the phenotype includes a small eye, which is not reported in human patients (Kokotas and Petersen, 2010). Rat *Small-eye* mutations (*rSey* and *rSey*^{2}) cause a similar phenotype (Matsuo et al., 1993; Osumi et al., 1997). Both mouse and rat *Small eye* mutations result in premature stop codons. Other missense mutations in the mouse are hypomorphs with varying degrees of different eye abnormalities (Favor et al., 2008, 2001). Homozgyous null mutations are lethal in mice, with severe brain and olfactory deficits (Hogan et al., 1986), and in the rare cases of compound heterozygotes in humans most individuals die perinatally (Glaser et al., 1994).

The *Pax6* gene has a complex structure and regulation (Shaham et al., 2012) that reflect the many functions of this gene and which are relevant to the mutations discussed in this study. The gene has 16 exons, and three promoters drive its expression yielding several transcripts. Transcription is further controlled by a large number of regulatory elements that reside both within the gene and at significant distances 5′ and 3′ of the coding region. Details relevant to this paper are described in Fig. 1 and discussed in the Results section. This transcription factor has the characteristic structural features of many genes in the *Pax* family, including the bi-partite DNA-binding paired domain toward the 5′ end of the gene, found in all members of this gene family. The paired domain is connected to a glycine-rich linker bridging it to a paired-like homeodomain. At the C-terminal end of the protein is a proline-serine-threonine (PST) domain that is essential for the transactivation properties of Pax6. The mouse *Pax6*^{Sey} mutation described above is due to a nonsense mutation upstream of the 5′ end of the homeodomain and is presumed to be a null mutation based on the fact that it is allelic to Dickie's *Small eye* (*Sey*^{Dey}), which deletes the *Pax6* gene (Hogan et al., 1988) and generates an identical phenotype to *Sey*^{Dey} in homozygotes. Similarly it is presumed that in human aniridia the *PAX6* gene is likewise generally a null since it presents with the same aniridia phenotype in WAGR (*W*ilms tumor, *a*niridia, *g*enitourinary abnormalities, mental *r*etardation) syndrome that occurs because of a chromosomal deletion that includes the *PAX6* gene (Prosser and van Heyningen, 1998).

Some embryonic gene targets of *Pax6* that may result in the numerous phenotypes described above have been studied but significant questions remain, particularly about the earliest changes in targets associated with *Pax6* mutations, but also those associated with later events, including brain development and later eye defects. In *Xenopus*, *pax6* is activated at the late gastrula stage in the presumptive anterior neural plate and is continuously expressed thereafter (Hirsch and Harris, 1997), a pattern seen in mammals as well. In the mouse, following neurulation, a member of the *Necab* gene family (N-terminal EF-hand calcium binding proteins) is downregulated in the *Sey* mutant but a number of key regulatory genes important in retina and forebrain formation that have been examined at this stage of development (e.g. the homeobox genes *Six3*, *Otx2*, *Rax* and *Lhx2*) were not found to be immediate targets of *Pax6* (Bernier et al., 2001). Nuclear protein gene *Mab21l1* (Yamada et al., 2003) and the secreted frizzled-related protein gene *Sfrp2* (Wawersik et al., 1999) are also downregulated in the *Sey* mutant. In a zebrafish study of *pax6* targets (Coutinho et al., 2011) a number of genes are downregulated upon morpholino antisense oligonucleotide treatment of embryos and studies on specific differentiated tissues in the mouse, e.g. the lens,

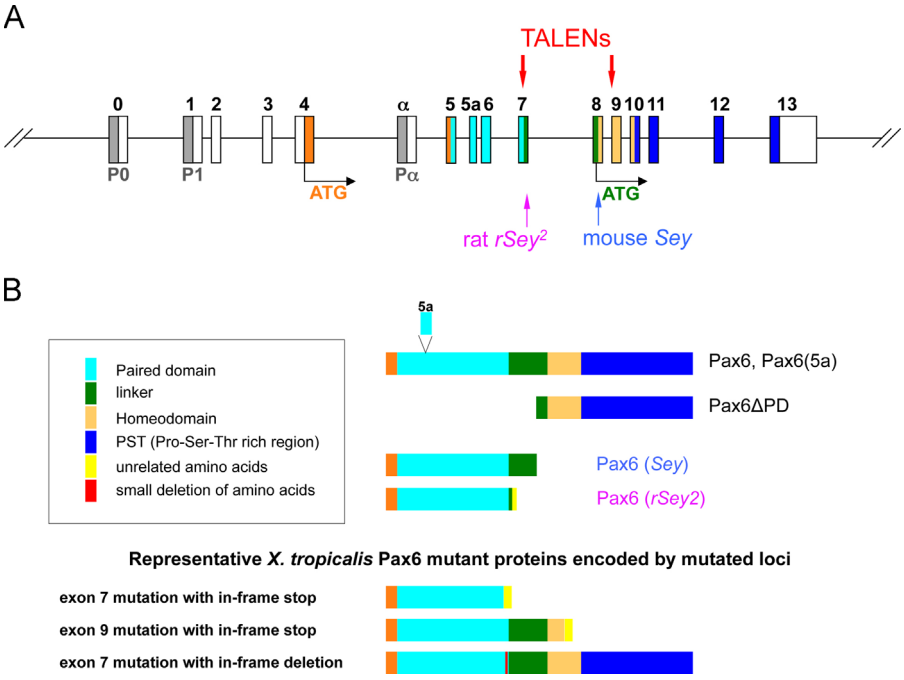

Fig. 1. Strategy for targeted mutagenesis of *Xenopus tropicalis pax6* locus. (A) Structure of *pax6* gene is shown schematically (not to scale). P0, P1, Pα are promoters (shaded in grey). Exons (boxes) are numbered or named on top (0 to 13 or α) and color coded: white, untranslated regions (UTRs); orange, N-terminal region before the paired domain; other colors correspond to color codes for protein domains shown in (B). Two translation start sites are shown (ATG): orange, for full-length isoforms (Pax6 with or without 5a); green, for paired-less isoform (Pax6ΔPD). Positions of mouse *Sey* and rat *rSey*^{2} mutations are indicated by arrows on the bottom. Two pairs of TALEN targets in exon 7 and exon 9 are shown on top. (B) Structures of Pax6 wild-type and representative mutant proteins are shown schematically (not to scale). Color codes of protein domains are shown in the box except the first three amino acids, which are shown in orange. Note that the paired domain is located between amino acids 4–131 and the homeodomain between amino acids 212–272 in *X. tropicalis* due to insertion of two amino acids between the two domains. The amino acid sequence of each domain is as shown in Walther and Gruss (1991). Most but not all mutations have some non-Pax6 amino acids at the C-terminus. Note that *X. tropicalis* mutations in exon 7 could theoretically encode Pax6ΔPD if mutations were not simultaneously introduced in exon 9 (not shown in the drawing). (For interpretation of the references to color in this figure legend, the reader is referred to the web version of this article.)

provide a more global analysis of later *Pax6* targets (Wolf et al., 2009). However there remains very little information about the changes in gene expression, and their effects on development, that accompany the period just after *Pax6* activation at the end of gastrulation and during early neurula stages when important elements in patterning of the retina and neural plate are being established (Saha and Grainger, 1992).

The rapid progress in gene editing with TALEN and CRISPR constructs in the past few years (Peng et al., 2014) has allowed rapid genetic manipulations in *Xenopus* as in many other organisms. Both TALENs (Ishibashi et al., 2012; Lei et al., 2012; Nakajima et al., 2013; Nakajima and Yaoita, 2013) and CRISPRs (Blitz et al., 2013; Guo et al., 2014; Nakayama et al., 2013) have generated mutant phenotypes in a number of genes and genetically modified lines in the case of production of albino animals mutated in the *tyrosinase* gene. The study described here, in which we target the *pax6* gene with TALEN constructs, is the first in depth study in which F1 and/or F2 non-mosaic animals carrying putative mutations in a key developmentally regulated gene have been examined using targeted gene editing in *Xenopus*. A previous study described the F0 mosaic phenotype in *Xenopus laevis* embryos where the *pax6* gene was targeted (Suzuki et al., 2013).

In this study we find that gene targeting of *pax6* results in a highly consistent, putative null phenotype in F1 and F2 homozygote and/or compound heterozygote embryos: a severely reduced eye which fails to form a lens. The consistent mutant platform permits us to begin to examine gene expression changes that accompany the initial phases of retina and brain formation and provides a powerful starting point for elaborating the initial functions of the *pax6* gene during development. An allele was also identified that appears to reduce but not inactivate *pax6* activity, revealing a hypomorphic phenotype in which early development appears normal but froglets exhibit eye abnormalities very similar to those seen in aniridia patients, providing a highly accessible model system for studying the ontogeny leading to the aniridia syndrome and for potentially mitigating the disease phenotype.

Materials and methods

Construction of TALENs to target the pax6 gene

TALEN scaffolds with the obligate heterodimeric FokI (ELD/KKR) were obtained from Christopher H. K. Cheng (pCS2+TALEN-ELD/KKR; (Lei et al., 2012). For an experimental control, we used pCS+TALEN-ELD/KKR-Tyr I (to target the *tyrosinase* gene), which was described previously (Nakajima and Yaoita, 2013), hereafter referred to as pCS-ELD/KKR-Tyr I for simplicity. To target exon 7 and exon 9 of the *pax6* gene, we chose 5′-GTCATCAATAAACCGAGTGCTGCGCAACCTGGCGAGC-GAAAAGCA-3′ for exon 7 and 5′TTGAACGAACACATTACCCCGACG-TGTTTGCCAGGGAAAGATTAGCTGCC-3′ for exon 9, where underlined sequences are left targets and double-underlined sequences are right targets (in antisense-strands). The DNA binding domains to recognize these targets were assembled as previously described (Cermak et al., 2011) with minor modifications as reported (Nakajima et al., 2013). TALENs recognizing left targets were constructed in pCS+TALEN-ELD to yield pCS+TALEN-ELD-pax6 E7 (for exon 7) or E9 (for exon 9), and pCS+TALEN-KKR-pax6 E7 or E9 were similarly constructed for right targets. Hereafter these are referred to as pCS-ELD/KKR-pax6 E7/E9 for simplicity. The EMBOSS program fuzznuc (Rice et al., 2000) was used to search for possible off-target sites of these TALENs based on the *X. tropicalis* genome sequence Assembly v4.1 (Hellsten et al., 2010). Since the repeat variable di-residue NN for recognizing the nucleotide G could also bind to the nucleotide A, R (i.e., G or A) was used in the off-target search of left targets and Y (i.e., C or T) in the right targets search. Thus the off-target sites of pCS-ELD/KKR-pax6 E7 used both the sense 'RTCATCAATAAACCRN(10,30)GGYGAGYGAAAAGYA' and the antisense sequence 'TRCTTTTCRCTCRCCN(10,30)YGGTTTATTGATGAY', ELD/KKR-pax6 E9 used 'TTRAACRAACACATTN(10,30)YYAGGGAAAGAT-TAGYTGYY' and 'RRCARCTAATCTTTCCCTRRN(10,30)AATGTGTTYGT-TYAA', and pCS-ELD/KKR-Tyr I used 'TTCTTCTTCCTCCATRTN(10,30) YYYAAGGGYATGTAGYA' and 'TRCTACATRCCCTTRRRN(10,30)AYATG-GAGGAAGAAGAA'. Since TALENs from pCS-ELD-pax6 E7 and pCS-KKR-pax6 E9 or pCS-ELD-pax6 E9 and pCS-KKR-pax6 E7 could make a heterodimer when 4 TALEN mRNAs are co-injected, we also tested combinations of the exon 7 left target and the exon 9 right target, 'RTCATCAATAAACCRN(10,30)YYAGGGAAAGATTAGYTGYY' and 'RRCARCTAATCTTTCCCTRRN(10,30)YGGTTTATTGATGAY', as well as the exon 9 left target and the exon 7 right target, 'TTRAACRAACA-CATTN(10,30)GGYGAGYGAAAAGYA' and 'TRCTTTTCRCTCRCCN(10,30) AATGTGTTYGTTYAA'. We saw a few theoretically possible off-target sites with 10 to 30 spacer nucleotides having three or more mismatched nucleotides, but no complete matches to off-target sites were found in any of the combinations examined.

Xenopus tropicalis, synthesis of TALEN mRNAs and microinjection

We used in house breeding stocks of *X. tropicalis*, which are not highly inbred but originated from the same ancestors of the Nigerian inbred line that was used for genome sequencing (Hellsten et al., 2010). *X. tropicalis* eggs were fertilized *in vitro*, dejellied, and injections made into one cell stage embryos within 40 min after fertilization as in earlier studies (e.g. Ogino et al., 2006). Embryos were raised to adults as described previously (Hirsch et al., 2002).

The capped mRNAs encoding each TALEN that were injected into embryos were synthesized from pCS-ELD/KKR-Tyr I and pCS-ELD/KKR-pax6 E7/E9 using the mMESSAGE mMACHINE® SP6 Kit (Invitrogen). A pair of each 100 pg or 200 pg of TALEN mRNAs for left and right targets was mixed for injection. As for dual targeting exon 7 and exon 9 simultaneously, two pairs of TALENs (each 100 or 200 pg) were mixed and injected.

Genotyping of pax6 and rax mutant and wild-type embryos

Since we can easily distinguish between *pax6* "null" mutant and wild-type phenotypes at tadpole stages due to different morphologies of the eye region, we do not necessarily perform genotyping on embryos older than st.35 [all stages according to Nieuwkoop and Faber (1994)]. In this case, the genotype of embryos with a wild-type appearance is designated as (+/?). All embryos shown at earlier stages were genotyped. Embryos were lysed as described (Fish et al., 2012), followed by genomic PCR of the *pax6* region (PCR primers are listed in Fig. 3). The PCR amplicon was purified and sequenced, or as needed, re-cloned and sequenced. In most experiments, phenotypes are indistinguishable between +/+ and +/−, and thus one representative embryo of either genotype has been chosen as a "wild-type" exemplar to image and labeled as (+/?) unless otherwise described. Genotyping of *rax* mutant and wild-type embryos was performed as described (Fish et al., 2014).

Tissue processing and histology

For *X. tropicalis* studies, to analyze mutant phenotypes, embryos were fixed overnight in Bouin's fixative and embedded either in JB-4 Plus® resin (Polysciences) or in Paraplast® Plus. Plastic embedded tissue was sectioned at 3 μm and stained with toluidine blue. Paraffin embedded tissue was sectioned at 10 μm and stained with hematoxylin. For assessing expression domains of certain transcription factors following *in situ* hybridization,

some embryos were supported in a clay dish and sliced with a small scalpel.

For preparation of human corneal samples, tissues were placed in 4% paraformaldehyde and stored at 4 °C. For mouse samples, immediately after euthanization (CO_2 and cervical dislocation), both eyes from mice were enucleated and immersed in Davidson's fixative (Poly Scientific R&D Corp. Bay Shore, NY) at room temperature for 24 h. The eyes were then rinsed briefly in water and then transferred into 10% neutral buffered formalin for storage. Mouse globes were measured (Castroviejo calipers) at the horizontal equator using 2.5 × magnification. Both mouse globes and human corneal tissues were hand-processed and embedded in paraffin wax according to the following protocol: 70% ethanol for 30 min, 3 × 100% ethanol for 30 min, 2 × xylene for 30 min, 3 × 100% wax (Surgipath Paraplast, Leica) for 30 min at 62 °C. For mouse eyes, 7 μm sagittal sections one quarter of the way into the globe based on prior measurements were made using a rotary microtome; sections from human corneas were cut at 10 μm. Sections were captured on SuperFrost Ultra Plus slides. For routine microscopy, sections were then deparaffinized in two changes of xylene, rehydrated in graded ethanol (100%, 100%, 95%, 95%, and 70%), rinsed in water, stained with 10 min each of Gill II Hematoxylin (Surgipath™, Richmond, Il.) and Eosin (Surgipath™, Richmond, Il.), followed by a dehydration in graded ethanol (70%, 95%, 95%, 100%, 100%) and then two changes of xylene. Upon completion of staining, a coverslip was applied with Cytoseal 60 (Richard-Allan Scientific).

In situ hybridization

Whole-mount *in situ* hybridization was carried out essentially according to the procedure in Sive et al. (2000), though modified when genotyping was required, omitting acetic anhydride and post-color fixation steps as described (Fish et al., 2014). A minimum of 3 (up to 5) mutant embryos were examined by *in situ* hybridization for alteration of expression of downstream genes, showing highly consistent results. All antisense probes were labeled with digoxigenin (Roche) and detected by BCIP/NBT (Roche) or BM Purple (Roche). Probes for *myc* and *pax6* were prepared as described previously (Fish et al., 2014). *mab21l1* cDNA in pCS107 vector was obtained from The Wellcome Trust Sanger Institute and digested with *Eco*RI and used as template for T7 *in vitro* transcription to make the probe. Probes for *ins*, *gsx2*, and *neurog2* were made from templates created by genomic PCR as described (Fish et al., 2014). Primers used for these probes are as follows (5′ to 3′ direction, underlined nucleotides indicate T7 sequences):

ins 5′ primer, CCAGGACAACGAGTTGGATG
ins 3′ primer, TAATACGACTCACTATAGGGAGAAGCTCTTCAGCTTACATTTATTTGC
gsx2 5′ primer, CTGCGGCAATGTCTAGGTCT
gsx2 3′ primer, TAATACGACTCACTATAGGGAGATCATGCAATGGAATCTCCTG
neurog2 5′ primer, ACTGCCATCATTACCCGAAG
neurog2 3′ primer, TAATACGACTCACTATAGGGAGAGCACAGAGAAAGGCAACACA

Frogs

The frogs used for this study were from our colony maintained at the University of Virginia. All procedures involving frogs were performed in accordance with the National Institutes of Health Guide for the Care and Use of Laboratory animals and approved by the University of Virginia Animal Care and Use Committee.

Mice

The mice used for this study were maintained as a *Pax6*$^{Sey\text{-}Neu/+}$ colony on a majority CD1 genetic background with enough C57BL6/J to provide iris pigmentation. Wild-type (*Pax6*$^{+/+}$) littermates were used as controls. The genotype of each animal was determined by PCR as previously described (Kim and Lauderdale, 2006). All experiments involving mice were conducted in strict accordance with the National Institutes of Health Guide for the Care and Use of Laboratory Animals and were performed with approval and oversight of the University of Georgia Institutional Animal Care and Use Committee.

Human tissues

Cadaveric *PAX6*-normal human corneoscleral tissues derived from consented donors according to Institutional Review Board (IRB)-approved protocols were obtained from the Georgia Eye Bank. Aniridia tissue derived from consented donors according to Institutional Review Board (IRB)-approved protocols were obtained from Dr. John M. Freeman (Memphis Eye and Cataract Associates, Memphis, TN); tissue was obtained as byproduct of scheduled procedures.

Results

Strategy for targeted mutagenesis of Xenopus tropicalis pax6 gene and resultant mutations

As discussed earlier, the *pax6* gene locus has a complex structure (Fig. 1A), i.e., there are three promoters (P0, P1 and Pα) and alternative splicing events to create different mRNAs, some of which encode the same protein(s), and others which can create different protein(s). Translation is initiated at the ATG in exon 4, to yield a full-length protein, or at the ATG in exon 8 to yield a paired-less protein (Kim and Lauderdale, 2008). Although to date only one cDNA for *X. tropicalis* has been reported (i.e., NM_001006762) which lacks the exon 5a (used in one alternative spliced form; illustrated in Fig. 1B) and encodes a 424 amino-acid protein, there are EST clones containing exon 5a (e.g. CR438572). In a previous study we showed evidence that promoter α appears to be functional in *X. tropicalis* (Fish et al., 2012), suggesting that in *X. tropicalis* there must also be multiple versions of Pax6 mRNAs and proteins being expressed. Widely studied mouse and rat mutations are thought to be null mutations: the mouse *Pax6* mutant *Sey* has a substitution in exon 8 that creates a premature stop codon (Hill et al., 1991), and rat *rSey*^{2} has an insertion in exon 7 (Osumi et al., 1997) to create (downstream) an in-frame stop codon (Fig. 1B). In order to create similar null mutations in *X. tropicalis* and knock out the function of proteins resulting from both start sites the following strategy was undertaken: to block or inactivate proteins from the first ATG (Fig. 1A), we designed a target in exon 7 using TALENs as shown schematically in Fig. 1, and to block all protein forms, including the paired-less protein (Pax6ΔPD) derived from the second ATG, we also targeted exon 9.

We injected mRNAs for a pair of TALENs to target exon 7 and a pair of TALENs to target exon 9 individually or simultaneously. We also tested a pair of TALENs to target *tyrosinase* (*tyr*) (Nakajima and Yaoita, 2013) as a positive control for the experimental procedure as well as a negative control for morphological phenotypes that may be caused by the injection of any TALENs. Since our ultimate purpose was to establish mutant lines, we did not necessarily score F0 embryos systematically. However, at both doses we tested (100 pg or 200 pg of each TALEN mRNA), we observed morphologically abnormal eyes in *pax6* TALENs-injected embryos (Fig. 2).

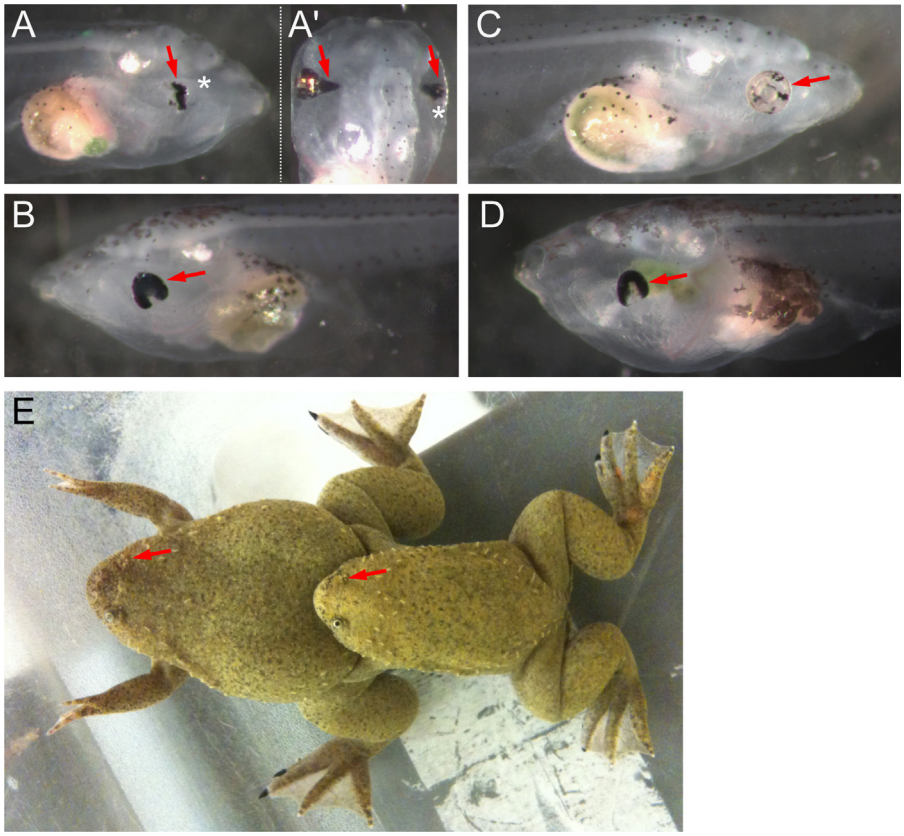

Fig. 2. Representative phenotypes of F0 embryos injected with TALENs. Lateral (A and B) and dorsal (A′, the same embryo shown in A) views of two embryos injected with a pair of TALENs targeting *pax6* exon 9 (200 pg mRNA each). Asterisks in (A) and (A′) indicate the same abnormal eye. The most frequently seen eye phenotype is shown in (B) (arrow). (C) Lateral view of an embryo injected with a pair of TALENs targeting *tyr* (200 pg mRNA each). The eye is morphologically normal but less pigmented (arrow). (D) Lateral view of an embryo injected with two pair of TALENs targeting *pax6* exons 7 and 9 (200 pg mRNA each). The abnormality here (arrow) is similar to what is shown in (B). (E) Mating of mature frogs raised from embryos injected with two pairs of *pax6* TALENs. Eyes are missing in one side of each animal (arrows).

The most frequent eye phenotype seen at tadpole stage is a horseshoe-shaped retina as seen from a lateral view, i.e., the ventral part of the eye is not formed (Fig. 2B and D). Although F0 animals sometimes had more severely degenerated eyes (Fig. 2A, lateral view), this degree of abnormality was not seen in F1 non-mosaic mutant animals (F1 mutants will be described in more detail later). Another interesting feature of mutants apparent when viewing animals from the dorsal aspect was a variable disturbance of the transformation of the initially broad connection between the brain and optic vesicle/cup, i.e. the optic stalk, into the optic nerve. In some, but not all, phenotypic F0 animals the optic stalk would persist in the form of a broad, cone-shaped extension of the retinal tissue spanning part (Fig. 2A′, left eye), or all (see example in Fig. 5 for F1 animals), of the distance between the eye and the brain. By contrast, *tyr* TALENs-injected embryos had eyes with variably reduced pigmentation which were otherwise morphologically normal as expected (Fig. 2C).

It is important to note that the dual targeting of exons 7 and 9 simultaneously can, in addition to creating deletions within exon7 or exon 9, create 10-kbp inversions or deletions between exons 7 and 9. This was demonstrated by a genomic PCR assay using different combinations of primer sets to amplify each exon, making it possible to detect deletions spanning exon 7 and 9 and inversions of the region between exon 7 and 9 (see Fig. 3A and B). We further focused on examining the 10-kbp deletion event by cloning and subsequent sequencing of genomic-PCR fragments to verify the existence of this large deletion, demonstrating that both pairs of TALENs had indeed cut simultaneously resulting in the large deletion (Fig. 3C). Although we did not sequence other PCR fragments individually from other F0 embryos, this result suggested that small indels in exon 7 and/or exon 9, and 10-kb inversions were likely occurring in many mosaic F0 embryos injected with both pairs of TALENs, which we confirmed in F1 animals (see below). Embryos (injected with both exons 7/9 TALENs together and exon 9 TALENs alone) that had abnormal eyes but which were otherwise normal in appearance were sorted and raised to adults (Fig. 2E) to establish F0 populations. We hypothesized that animals with an abnormal or missing eye would likely be mosaics with a high level of mutations in part of the animal but which were viable because other regions were either wild-type or had non-lethal (heterozygous) mutations. The stock 716 population (st.716) is comprised of F0 frogs targeting both exons 7 and 9, and the st.718 population targets exon 9 alone.

Germline transmission of mutations and establishment of lines carrying pax6 gene mutations

Germline transmission of mutations in mosaic F0 frogs was evaluated by generating F1 animals from matings of F0 adults (as illustrated in Fig. 2E). In crosses of these F0 frogs we observed mutant phenotypes in the resulting compound heterozygote F1 animals, as described in more detail below, similar to what we saw in F0 animals, verifying germline transmission of the mutations. We then systematically outcrossed F0 frogs with wild-type frogs to assay for germline transmission frequencies and allelic variation. All six of the st.716 frogs tested had germline transmission at various frequencies (notably, male frog #3 had 100% germline transmission of mutations), whereas only three out of seven st.718 frogs tested had germline transmission. The mutation profiles and their frequencies are summarized in Supplementary data Table S1.

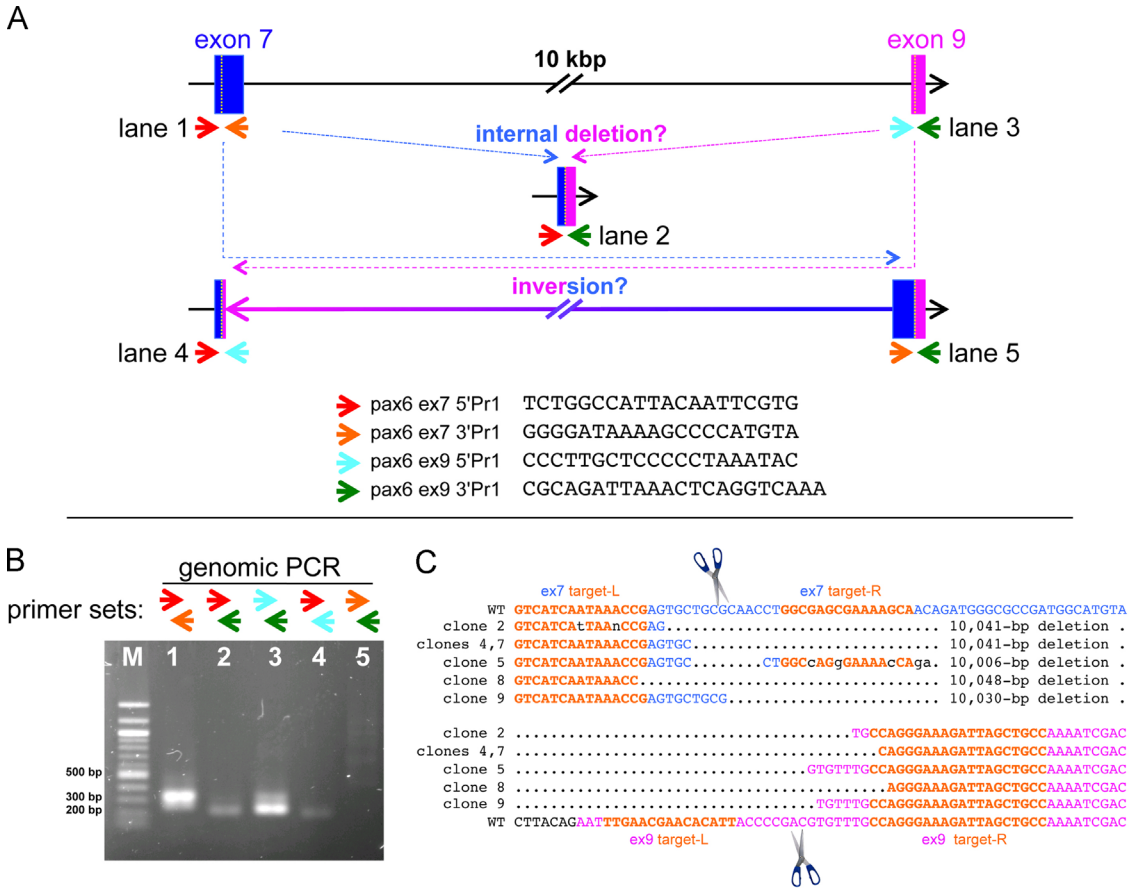

Fig. 3. Strategy for screening mutations in the *pax6* locus edited by two pairs of TALENs targeting exon 7 and exon 9 simultaneously. (A) Schematic drawing of targeting regions, only showing exon 7 (blue) and exon 9 (magenta) for simplicity (not to scale). Small colored arrows indicate different primers for genomic PCR of exon 7 and exon 9 (each sequence is shown on the bottom, from 5′ to 3′). Different combinations of primers can amplify other possible junction regions created by deletion or inversion between exons 7 and 9 as schematically shown. (B) A representative gel pattern of genomic-PCR bands from an embryo injected with both pairs of TALENs mRNAs. In this specific case, one of the possible junctions representing a 3′ inversion site (where a 3′ piece of exon 7 would have been fused inverted to 3′ piece of exon 9, lane 5) was not detected, but in other cases, we have seen such a band. (C) The genomic-PCR band corresponding to what is shown in lane 2 in (B) from 3 pooled embryos was gel-purified, cloned, and sequenced. The results of 6 clones are aligned. Only regions between two target sites (target-Ls, left target; target-Rs, right target in orange) are shown. Corresponding wild-type sequences are shown on top for exon 7 and on the bottom for exon 9. Multiple 10-kb deletion events were confirmed, and junctions where 5′ parts of exon 7 (blue) fused to 3′ parts of exon 9 (magenta) were seen in the expected cleavage regions (in between left and right targets, indicated by scissors) in both exons 7 and 9, suggesting that 10-kbp deletions were due to cleavages by TALENs and thus both TALENs were functional. (For interpretation of the references to color in this figure legend, the reader is referred to the web version of this article.)

To date, we have not yet confirmed germline transmission of 10-kbp deletions between exons 7 and 9, but we have confirmed at least one 10-kbp inversion between exons 7 and 9. Others are small (up to 17-bp deletion) indels created in exon 7 or exon 9 alone, or simultaneously in both exons, which in many cases cause frameshifts, resulting in premature stop codons. The predicted protein products are schematically shown in Fig. 1B (bottom). As a consequence, such mutations in exon 7 encode proteins truncated after amino acid positions between 125 and 128 depending on the individual mutation, thus lacking a few amino acids at the end of the paired domain (that is located between amino acid residues 4–131) and the remainder of the coding sequence. Exon 7 mutants could still theoretically encode the Pax6ΔPD isoform if mutations were not simultaneously introduced in exon 9. Out-of-frame mutations in exon 9 encode proteins truncated after amino acid positions between 236 and 239 depending on the individual mutation, thus lacking amino acids after the middle of the homeodomain (located between amino acid residues 212–272). As we describe below, these mutations seem to behave as null mutations and the proteins, if they are expressed, do not seem to be functional.

In some cases, small indels created in-frame deletions of [3 × *n*] bp to result in 1–5 amino-acid deletions without changing the remainder of the protein. In case of exon 7, 1 to 5 amino acid deletions are found in the region between 125 and 129 of the paired domain, whereas in exon 9, one case shows a deletion of amino acid 238 in the homeodomain. We do not know at this time if one amino acid deletion due to the in-frame exon 9 mutation has any impact on the mutated protein function. However, we do see an impact of small in-frame deletions in exon 7 on the resultant protein, discussed in detail below.

Several outcrossed F1 animals were raised to adults, establishing F1 heterozygous frogs that have small indels in either exon 7 or 9, or in both, and one F1 heterozygous frog that has a 10-kb inversion between exons 7 and 9. Both F0 and F1 mutant carriers are used in this study. Several F2 lines are now being raised for future study.

Consistent phenotypes are seen in mutants with premature stop codons in exon7, or combinations of mutations in exon 7 and exon 9

The various induced *pax6* mutations leading to frameshifts and resulting in premature stop codons are expected to abrogate gene activity, particularly the exon 7 target site. As expected we find that there is a consistent phenotype in compound heterozygous or homozygous frameshift mutations in exon 7. But in addition we see an identical phenotype in all combinations examined of compound heterozygotes involving exon 7 and exon 9 out-of-

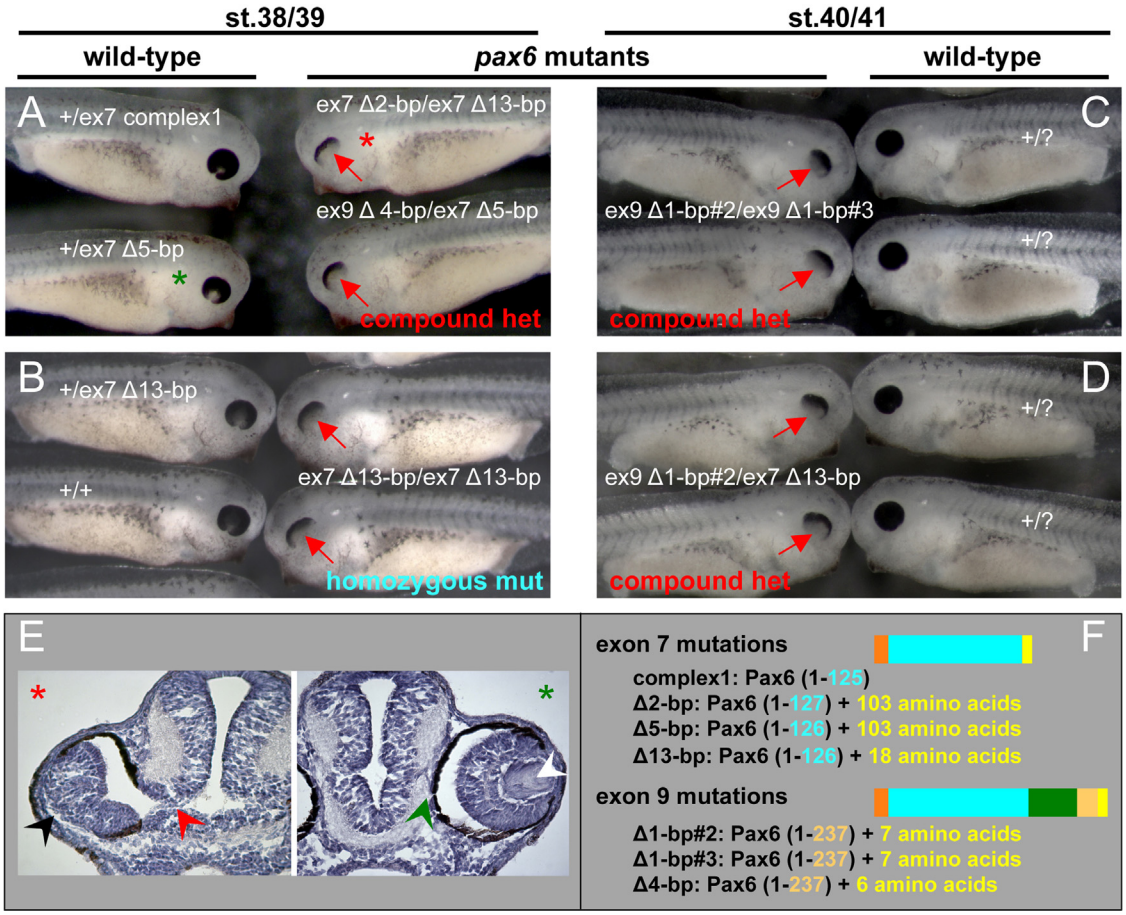

Fig. 4. *Xenopus pax6* mutants have abnormal eyes without lenses. (A–D) Offspring from crosses between F0 mosaic mutation carriers (A) or F1 carriers (B–D) showed a consistent phenotype in the eye (red arrows) regardless of the genotype of mutant alleles. F0 crosses (st.716 female #2 x male #3) created a variety of combinations of genotypes in mutant offspring (A), whereas 25% of offspring from F1 crosses (i.e., parents are not mosaic) have a single homozygous (B) or compound heterozygous (C,D) mutant genotype as expected. Note that mutants homozygous for a 13-bp deletion in exon 7 (B) are indistinguishable from other compound heterozygous mutants, regardless of the combination of exon 7 mutations (A, top right embryo), combination of exon 7 and exon 9 mutations (A, bottom right embryo and D), or combination of exon 9 mutations (C). Each embryo shown here was genotyped except for phenotypic wild-type embryos in C and D, thus shown as +/?. Judging from the mutation profiles (see Table S1), we could infer the origins of mutated alleles of offspring from F0 crosses, or in the case of F1 crosses, the genotypes of parents are known in advance, thus we show offspring genotypes in order of parental female locus/male locus except for the top wild-type embryo in (B), where the parental origin of alleles is undeterminable. Actual sequences of mutations can be found in Table S1. (E) Cross sections of embryos marked by red (mutant) and green (wild-type) asterisks in (A) to show morphology of the eyes. The wild-type embryo (green asterisk) has a lens (white arrowhead) and the retina is surrounded by retinal pigment epithelial (RPE) and separated from the brain (green arrowhead), whereas the mutant embryo (red asterisk) has no lens and the retina is disorganized (black arrowhead) and still connected to the brain (red arrowhead). (F) Schematic presentation of proteins encoded by the mutations shown here. Also refer to Fig. 1 for color codes. Exon 7 mutations cause truncation at the C-terminus of the paired domain (located between amino acid residues 4–131), whereas exon 9 mutations cause truncation in the middle of the homeodomain (located between amino acid residues 212–272). Truncations in many cases but not all are followed by unrelated amino acids due to the frameshift. Note that mutant embryos shown in (C) make almost identical mutant proteins with only one amino acid change at position 238, thus this is very close to being a homozygous mutation. (For interpretation of the references to color in this figure legend, the reader is referred to the web version of this article.)

frame mutants. Thus we hypothesize that both exon 7 and exon 9 mutations (and exon 7/9 deletions and inversions) yield inactive Pax6 protein. Fig. 4 (stage 38–41) and Fig. 5 (stage 42 and 47) summarize *pax6* mutant phenotypes of tadpoles from different matings of F0 and F1 mutant carrier frogs. The features of mutant embryos are consistent in any *pax6* mutant regardless of whether they are homozygous mutants that have the 13-bp deletion in exon 7 or compound heterozygous mutants, and regardless of whether mutations are in exon 7 or exon 9.

The first sign of a morphological phenotype in the mutant can be detected between late stage 20's to early stage 30's, but in some cases at such stages the phenotype is hard to distinguish from normal morphological variation in wild-type embryos (data not shown). The mutant phenotype becomes more obvious when pigmentation of the retinal pigment epithelium (RPE) is completed, i.e., at late stage 30's to early 40's. Surprisingly, *pax6* mutants in *X. tropicalis*, unlike *Pax6* mutants in mouse *Sey* (Hill et al., 1991) or rat *rSey*^{2} (Osumi et al., 1997) do not lose the eye completely, i.e., there is a persistent eye-like structure with an abnormal retina and no lens. As of stage 38–41 (Fig. 4), the mutant eye has a characteristic appearance showing the RPE only in the region corresponding to the anterior–dorsal side of the wild-type eye, and has a highly disorganized retina and no lens as seen in histological sections (Fig. 4E). As development proceeds (Fig. 5), the RPE acquires a flattened or arc shape because morphogenesis of the ventral optic cup fails (Fig. 5A and C, lateral views of mutants and Fig. 5E and F, transverse sections), a feature which was also observed in F0 mosaic embryos (Fig. 2B and D). In some cases, the RPE extends along the persistent optic stalk (Fig. 5A, B and C′, orange arrows) that contains differentiated retina tissue (Fig. 5E, red arrowhead).

Given that the rodent *Pax6* mutations that are similarly positioned to our frog mutations result in no or non-functional proteins (Engelkamp et al., 1999; Numayama-Tsuruta et al., 2007), it seems unlikely that the truncated protein(s) in the *X. tropicalis* mutants, if expressed at all, would be sufficiently functional to account for the

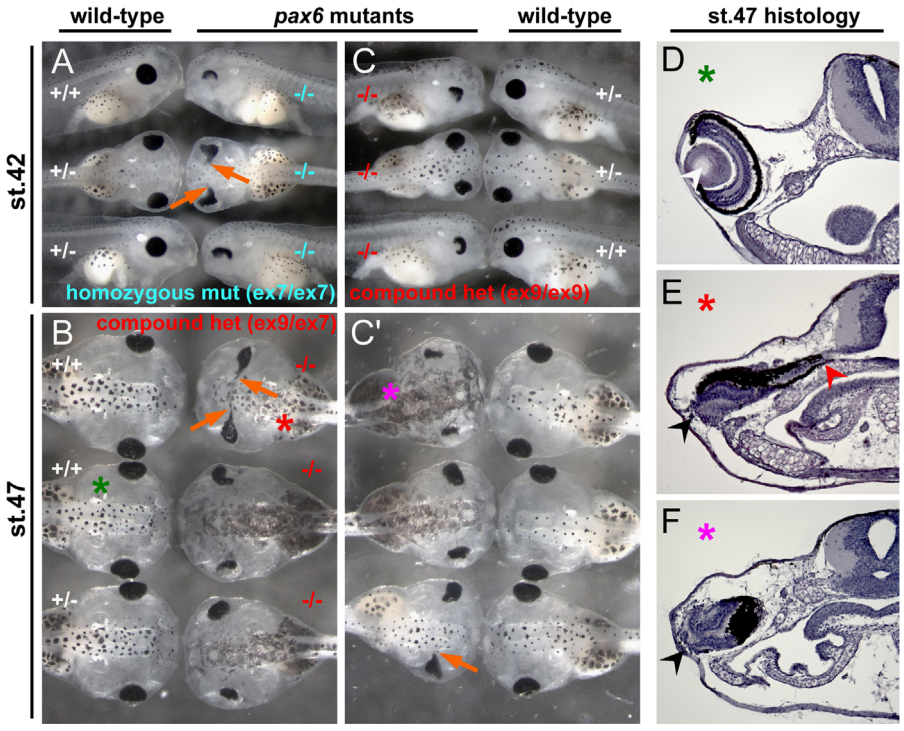

Fig. 5. Phenotypes of *Xenopus pax6* mutants at tadpole stages. (A) Phenotypes of F2 embryos at stage 42 from an intercross of F1 heterozygotes carrying a 13-bp deletion in exon 7. −/−, homozygous mutant; +/−, heterozygous; +/+, wild-type. These are siblings of embryos shown in Fig. 4B. (B) Phenotypes of F2 embryos at stage 47 from cross between an F1 female carrying a 1-bp deletion (#2) in exon 9 and an F1 male carrying a 13-bp deletion in exon 7. −/−, compound heterozygous mutant (genotype is ex9 Δ1-bp#2/ex7 Δ13-bp); +/−, heterozygous (genotype, +/ex7 Δ13-bp); +/+, wild-type. These are siblings of embryos shown in Fig. 4D. (C and C′) Phenotype of F2 embryos at stage 42 (C) and stage 47 (C′) from mating of an F1 female carrying a 1-bp deletion (#2) in exon 9 and F1 male carrying a 1-bp deletion (#3) in exon 9. Embryos shown in C (mixture of lateral and dorsal views) are the same embryos as shown in C′ (all dorsal views) at the same axial position, the only difference being their ages. −/−, compound heterozygous mutant (genotype is ex9 Δ1-bp#2/ex9 Δ1-bp#3); +/−, heterozygous wild-type (genotype, ex9 Δ1-bp#2/+ for top embryo, +/ex9 Δ1-bp#3 for second embryo); +/+, homozygous wild-type. These are siblings of embryos shown in Fig. 4C. Orange arrows show the eye fused to the brain, which is often, but not always, seen in *pax6* mutants regardless of genotype. (D–F) Cross sections of the eye region of embryos shown in (B) and (C′). Corresponding embryo and section are marked by the same colored asterisks. Wild-type embryos (D) have well organized retina and lens (white arrowhead), whereas mutants (E and F) do not have lens and the retina is disorganized (black arrowheads). By this stage, mutant eyes were separated from the brain in some embryos (F) or still connected to the brain in other embryos (E, red arrowhead). (For interpretation of the references to color in this figure legend, the reader is referred to the web version of this article.)

incomplete loss of eyes that we see. Rather, there is another possibility that a second *pax6*-related gene, *pax6.2*, may have redundant function in *Xenopus* embryos and may partially rescue *pax6* mutations. It was recently discovered that non-mammalian vertebrates all appear to have this second *pax6*-like gene and that the gene has been lost in birds and mammals (Ravi et al., 2013). *X. tropicalis* Pax6.2 (XM_004912020) consists of 281 amino acids and has 85% amino-acid identity with the region of amino acids 137–424 of *X. tropicalis* Pax6. It consists of the homeodomain and PST but no paired domain, as is characteristic of all *pax6.2* genes. To assess the possible overlapping role of *pax6.2* with *pax6*, we examined its expression by *in situ* hybridization (see Fig. S1). At early stages the expression is not detectable by *in situ* hybridization, but by stage 25 a low level of expression is detected in the dorsal half of the retina, and becomes more obvious at later stages. Expression at later stages is also seen in the notochord (*pax6* is not expressed in this tissue), and no expression is detected in the brain (again, unlike *pax6*). The *pax6.2* expression domain in the retina is coincident with the dorsal location where the partial retina is formed in *pax6* mutants, consistent with the possibility of involvement of *pax6.2* in ameliorating the *pax6* mutant phenotype in frog compared to mammals. Although evaluation of function of *pax6.2* in *pax6* mutants remains to be studied in the future, since all homozygous and compound heterozygous out-of-frame mutants involving exon 7 and 9 deletions show consistent phenotypes, at present we consider those phenotypes to result from in-frame, premature stop codons caused by indel-generated frameshifts (see Table S1) leading to protein products with no activity. These "null" mutant embryos at later stages have some axial defects (data not shown) and eventually die some time after stage 46. In the following analyses of the "null" phenotypes, we do not distinguish different mutated genotypes but simply regard embryos as falling into two classes: (1) frameshift mutations causing a premature stop codon (and a clear, consistent, embryonic phenotype); or (2) "wild-type" embryos with a normal appearance (but which may carry cryptic mutations).

Expression of genes downstream of pax6 at early and late stages during tadpole development

We have examined expression levels of several marker genes that are expressed in the same tissues and organs as *pax6* by *in situ* hybridization. Although more extensive studies will be performed in the future using homozygous mutant lines, in this initial study we focus on only a few genes. *Mab21l1* is a known downstream gene of *Pax6* and has important roles in eye development (Yamada et al., 2003). As expected and consistent with the report in mouse *Pax6* mutant (i.e., *Sey*/*Sey* (Yamada et al., 2003)), we also observed a reduction of expression of *mab21l1* in "null" *pax6* mutant frog embryos (Fig. 6A). We also tested *myc* expression that is known to be downstream of the key eye gene *rax* in the retina region (Fish et al., 2014) as shown in Fig. 6C, but has not been identified as a downstream target of *pax6* to our knowledge. We found that *myc* expression in *pax6* "null" mutant is indeed downregulated specifically in the regions where its expression overlaps with *pax6* (Fig. 6B), i.e., the retina and brain (red arrows) and presumptive lens ectoderm (PLE) at stage 15 (dotted white circles, Fig. 6D

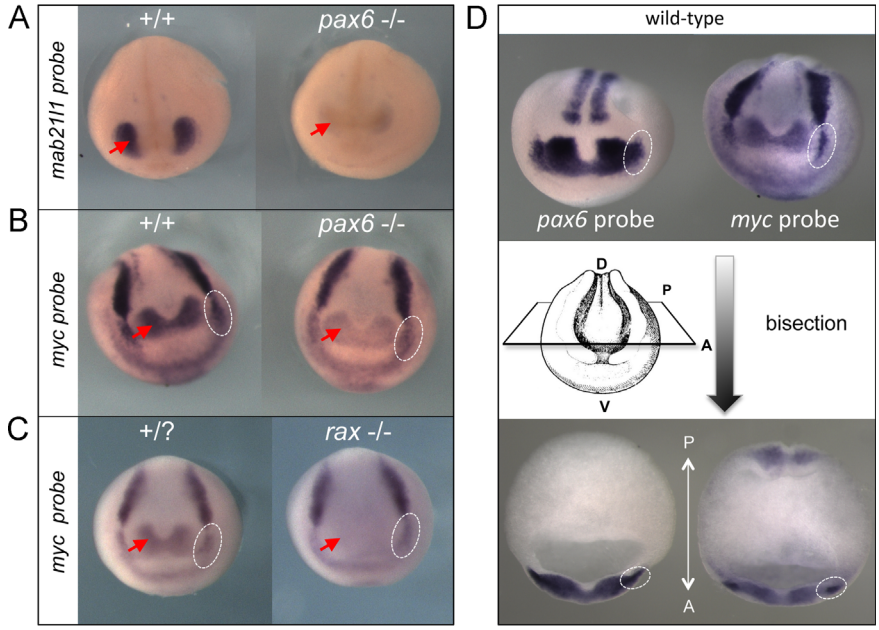

Fig. 6. *mab21l1* and *myc* are downstream of *pax6*. (A and B) *In situ* hybridization of wild-type (+/+) and *pax6* mutant embryos (−/−, compound heterozygote of complex1 and 10-kbp inversion mutations, see Table S1 for sequence) at st, 21 (A) or st. 15 (B) with *mab21l1* (A) or *myc* (B) probe. Red arrows indicate expression of *mab21l1* (A) and *myc* (B) in the eye region. Expression of both genes is reduced in mutants. (C) *In situ* hybridization of wild-type (+/?) and *rax* mutant (−/−, see Fish et al., 2014) embryos with *myc* probe. Note that *myc* expression in the presumptive retina region (red arrow) is almost completely lost in the *rax* mutant as reported previously (Fish et al., 2014), whereas in the *pax6* mutant *myc* expression is consistently reduced, but to a lesser extent as shown in (B). White dotted circles show the presumptive lens ectoderm (PLE) region, in which expression of *myc* is indistinguishable between wild-type and *rax* mutant embryos. By contrast, expression of *myc* in the PLE of *pax6* mutant is reduced compared to the wild-type embryo (B, white dotted circles). (D) *In situ* hybridization of wild-type embryos with *pax6* (top left) and *myc* (top right) probes at stage 15. The same embryos are bisected at the level shown schematically, clearly showing the expression of *pax6* and *myc* in the PLE (bottom, white dotted circles). (For interpretation of the references to color in this figure legend, the reader is referred to the web version of this article.)

shows both expression of *pax6* and *myc* in the PLE). This suggests that *myc* is downstream of both *rax* and *pax6*, and potentially plays a role in eye and brain development, and also that *myc* may be involved in lens development under the control of *pax6*.

While disruption of eye development is the most obvious effect of *pax6* mutation in frog embryos/larvae, examination of expression of a few genes involved with *pax6* in regulating regional forebrain development show that process to be compromised as well.

Although *pax6* function seems to be completely knocked out in our mutants, *in situ* hybridization reveals that the mRNA continues to be expressed throughout most of the normal expression domains. In the forebrain of late embryonic to larval stages of *Xenopus*, *pax6* is expressed in the pretectum (prosomere 1), dorsal thalamus (prosomere 2), prethalamus (prosomere 3) and in the telencephalon in the lateral and ventral pallium as well as in the lateral ganglionic eminence (lge) region of the subpallium and in the olfactory bulbs (Moreno et al., 2008). Interestingly, by stage 38 there is a clear loss of *pax6* mRNA from the pretectum and dorsal thalamus of mutants (Fig. 7A) also seen in mouse mutants (Mastick et al., 1997), suggesting that Pax6 protein must be required for continued expression in these regions.

To compare the effects of *pax6* mutations in our frog model with those described in *Pax6* mutants in other organisms, we looked at expression of a small number of genes either known to be *Pax6* targets or whose expression domain overlaps with that of *Pax6*.

Nkx2-1 is a homeobox gene that is essential for specification of the basal forebrain structure the medial ganglionic eminence (mge) (Sussel et al., 1999). In *Pax6* homozygous mutant mice, *Nkx2-1* expression expands laterally into the lge (Stoykova et al., 2000). Similarly, in frog *nkx2-1* is expressed in mge as well as the preoptic area and the hypothalamus (Gonzalez et al., 2002), and the mge domain appears to be expanded in our mutants (Fig. 7B).

Gsx2 (previously *Gsh2*) is another homeobox gene expressed in the developing vertebrate forebrain where, along with *Pax6* and *Nkx2-1*, it is known to play a key role in regional specification. In mice its primarily subpallial expression domain in the telencephalon is largely complementary to the mainly pallial domain of *Pax6*, but there is some overlap across the pallial/subpallial boundary (Yun et al., 2001). That these two genes act together to establish pallial vs subpallial territories is suggested by the observations that in *Pax6* mutant mice part of the ventral pallium is respecified into a structure with characteristics of lge, while in *Gsx2* mutant mice part of the lge is respecified into tissue with ventral pallium characteristics (Carney et al., 2009; Yun et al., 2001). Similarly, in *Xenopus gsx2* is expressed in the lge and in the prethalamus (Illes et al., 2009). Interestingly, when we looked at stage 41 the telencephalic expression of *gsx2* appeared similar in mutant and wild-type, however the prethalamic expression domain was missing in the mutants (Fig. 7C).

Lastly, we looked at expression of *neurog2*, another gene expressed during forebrain development and shown to be a direct target of *pax6* regulation (Holm et al., 2007; Scardigli et al., 2003). It is co-expressed in developing cerebral cortex (pallium) in mice, and its expression is reduced in *Pax6* homozygous mutant mice (Toresson et al., 2000; Yun et al., 2001). In the frog, the telencephalic (pallial) domain of *neurog2* expression appears to be reduced/missing in the *pax6* mutant (Fig. 7D), consistent with what has been observed in mouse *Pax6* mutants.

Although we have looked at only a few gene markers so far, we find alterations in gene expression patterns in the developing brains of *pax6* mutant frogs that are generally consistent with those predicted for downstream targets of *pax6* function and those reported in *Pax6* mutations in other organisms.

Finally, to expand our initial survey of sites of tissues where *pax6* is known to be essential, we looked for evidence of *pax6* malfunction in the developing pancreas where we examined

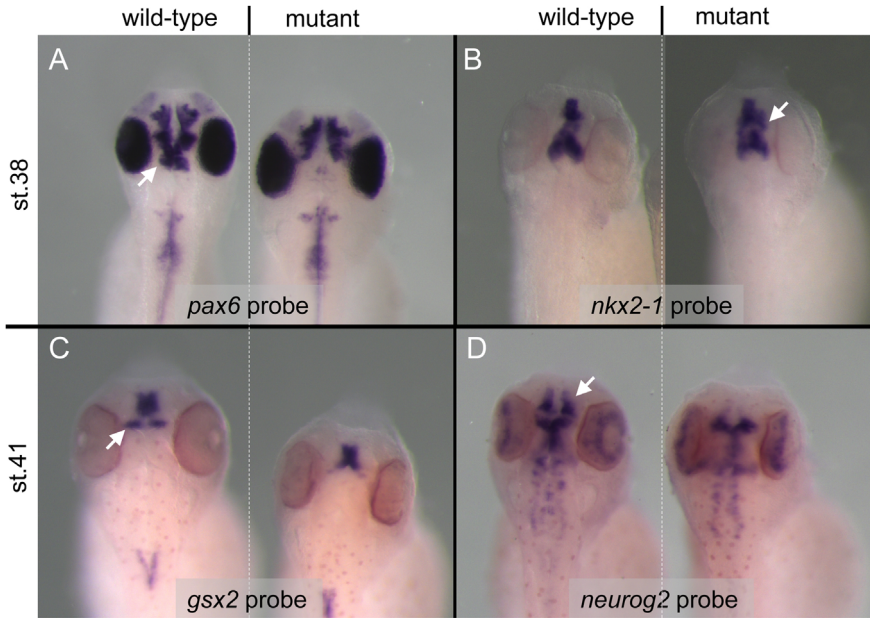

Fig. 7. *pax6* mutants display altered forebrain patterning. *In situ* hybridization comparison of expression patterns of several genes show altered brain patterns in mutant versus wild-type embryos. *pax6* mRNA expression is lost from the pretectum (white arrow) and ventral thalamus of mutants, but appears to be maintained normally in more anterior parts of the forebrain including retina at stage 38 (A). By contrast, as seen in panel (B) the expression domain of *nkx2-1* appears to be expanded in the telecephalon (white arrow) of *pax6* mutants compared to wild-type. *gsx2* expression is lost from the prethalamus (C, white arrow) of the mutant, and *neurog2* is greatly reduced in the telencephalon (D, white arrow) of mutant embryos.

insulin (*ins*) expression as an indicator of pancreas development, and as expected its expression was reduced in mutant embryos (Fig. 8), as has been reported in mouse *Pax6* mutants (Sander et al., 1997; St-Onge et al., 1997).

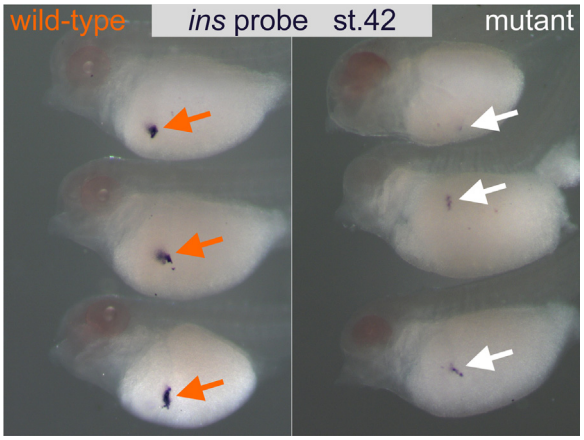

Fig. 8. *insulin* (*ins*) expression is downregulated in *pax6* mutants. Wild-type (left) and *pax6* mutant (right) embryos at stage 42 were subjected to *in situ* hybridization with an *ins* probe. Expression of *ins* gene in this lateral view of mutant embryos (white arrows) is reduced compared to the level seen in wild-type embryos (orange arrows). (For interpretation of the references to color in this figure legend, the reader is referred to the web version of this article.)

Hypomorphic alleles in combination with "null" alleles cause an eye phenotype similar to human aniridia

While establishing F1 lines, in one mating between F0 st.716 female #2 and male #3 we found a number of the offspring that developed into froglets which had a common abnormality, namely enlarged pupil size. These (total 12) froglets developed from the apparently wild-type 96 survivors of this mating, i.e. after those embryos showing the characteristic "null" phenotype (Fig. 4A) died during tadpole stages. That is, the froglets with the enlarged pupil phenotype appear to have had no distinctive embryonic phenotype. Fig. 9 shows typical gross morphological appearance of the mutant froglets. Genotyping of all 12 frogs (see Table S1) revealed that a specific combination of mutations was associated with what we postulate to be a hypomorphic genotype. All frogs have one allele with frameshifted mutations that encode truncated proteins lacking a few amino acids of the end of the paired domain and the rest of C-terminal portion of the Pax6 protein (as seen in "null" mutants). The other allele has an in-frame small deletion that deletes a few amino acids that in almost all cases includes arginine at amino acid 128 (R128), though in one case only amino acid residue 127 is deleted (see Fig. 9B left panel and Table 1) with the rest of the protein remaining intact. We hypothesize that this results in production of a Pax6 protein with reduced activity. We have recently confirmed that these froglets can survive, and some have reached sexual maturity. Thus, the features of their eye abnormality and the non-lethality of this condition are similar to what is seen in human aniridia patients. Because this mutation results in a phenotype that is significantly less severe than animals with two out-of-frame deletions (which are presumed to be null), we refer to the compound heterozygotes with an aniridia-like appearance as having a "hypomorphic phenotype."

Unlike human aniridia patients who commonly have no visible iris, all of the hypomorphic mutants have clearly visible, but substantially reduced iris tissue (Fig. 10). As in human patients, the eye phenotypes are somewhat variable among individuals and can even vary between the two eyes of one animal. Examination of hypomorphic and normal frog eyes revealed that the frog hypomorphic mutants show similar abnormalities as seen in humans including: most commonly, clear lenses (Fig. 10B and F), occasional focal cataracts (lens opacities) (Fig. 10C and G, white arrows), frequent peripheral clouding of the cornea (Fig. 10B, C and F, white arrowheads) and occasional focal losses of remaining iris tissue (Fig. D and H, red arrows). One hypomorphic mutant frog appeared to be missing one eye entirely, however upon dissection a very small rudimentary eye with retinal tissue was found beneath the skin (not shown).

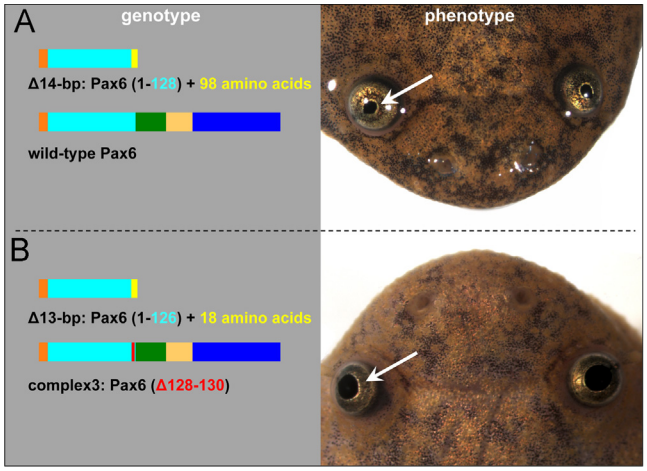

Fig. 9. Combination of truncated Pax6 protein and Pax6 protein with a small in-frame deletion causes an aniridia-like phenotype in *X. tropicalis* froglets. (A) An example of a heterozygous genotype (left) of phenotypically wild-type froglet (right). (B) An example of the compound heterozygous genotype (left) of an aniridia-like froglet (right). All other genotypes of aniridia-like froglets are listed in Table S1.

Table 1
Pax6 proteins encoded by mutations found in aniridia-like frogs.

Combination of proteins	Number of cases ($n=12$)
Pax6 (1–126)+additional 103 amino acids Pax6 (Δ128–130)	2
Pax6 (1–127)+additional 103 amino acids Pax6 (Δ128–129)	1
Pax6 (1–126)+additional 18 amino acids Pax6 (Δ127)	1
Pax6 (1–127)+additional 101 amino acids Pax6 (Δ128–130)	2
Pax6 (1–126)+additional 18 amino acids Pax6 (Δ128–130)	5[a]
Pax6 (1–125) Pax6 (Δ128–130)	1

[a] Their genotypes for in-frame deletions are in two patterns (9-bp deletion and complex3, see Table S1), but encode the same protein [Pax6 (Δ128–130)].

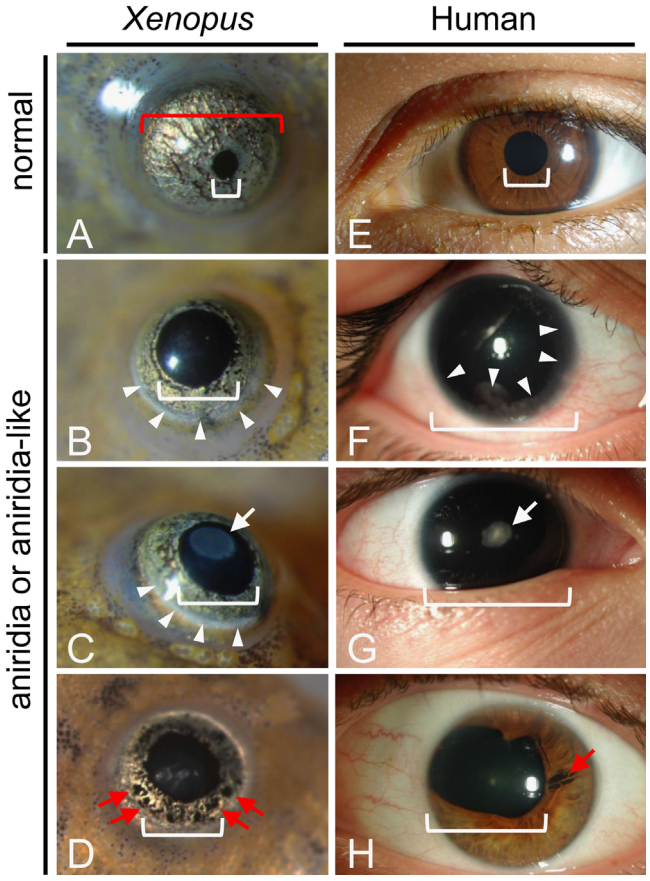

Fig. 10. Comparison of aniridia-like frog eyes with human aniridic eyes. For purposes of comparison the images of froglet eyes shown here are approximately half the size of the human eyes. Actual froglet corneal diameter is approximately one-tenth that of human. Normal frog (A) and human (E) eyes have small pupil (indicated by white brackets) and relatively large, pigmented iris. Aniridia-like mutant froglets (B–D) and human aniridia patients (F–H) show variable eye phenotypes including reduced (B–D, H) or absent (F and G) iris tissue. Remaining iris tissue may show focal losses (red arrows D and H). The lenses may be clear (B and F) or have a focal cataract (white arrows in C and G). Also, both frog and human eyes may show peripheral clouding of the cornea due to keratopathy (white arrowheads in B, C and F). (For interpretation of the references to color in this figure legend, the reader is referred to the web version of this article.)

Since the frog mutants generally retain some iris tissue, we made measurements of pupil diameter (Fig 10A, white bracket) and corneal diameter (Fig. 10A, red bracket) in our 12 hypomorphic mutants and 12 age-matched, wild-type froglets to better assess the degree of iris tissue reduction. We found that pupil diameter was about twice as large in mutant as compared to wild-type (0.63 $\pm$0.03 mm vs 0.34 $\pm$0.02 mm, $p=<0.0001$), while the overall eye size as represented by measurement of the corneal diameters was about 20% less in mutants compared to wild-type (1.22 $\pm$0.03 mm vs 1.46 $\pm$0.02 mm, $p<0.0001$) (Mean $\pm$ SEM, $n=24$ wild-type eyes, $n=23$ mutant eyes).

Histologic examination of three hypomorphic mutant frog eyes reveal several key features of the aniridia-like phenotype (Fig. 11) and permit further comparison with human aniridia and that seen in heterozygous *Pax6* mutant mice (Figs. 12 and 13). In overview, frog hypomorphic mutant eyes are somewhat smaller than normal, as indicated by the measurements described above, have lenses that are also slightly reduced in size (Fig. 11) and show abnormalities in both fiber cells and lens epithelium (Fig. 12). The corneas show abnormalities in layering (Fig. 13), and the irises are consistently reduced compared with normal (Fig. 11). In general, the hypomorphic eyes have well developed retinas although they may be folded, and the ganglion cell layer was sparse and irregular in the cases examined (Fig. 11), features also seen in some *Sey^{Dey}* mice (Theiler et al., 1978). In one case the retina was partially missing, but the remainder appeared normally developed (Fig. 11C).

To examine the phenotype in more detail, histological sections of the eyes from these animals were compared to wild-type frogs, 8-week-old wild-type adult mice and siblings heterozygous mutant for *Pax6* (Figs. 12 and 13). Because corneal defects are progressive in both individuals with aniridia and mice mutant for *Pax6*, young adult mice were chosen for these comparisons. The *Pax6$^{Sey\text{-}Neu/+}$* mice chosen for these experiments were on a majority CD1 genetic background to more closely model the genetics of human aniridia and selected for more normal eye sizes, again to more closely model human aniridia.

Like mice heterozygous mutant for *Pax6*, *Xenopus* harboring the hypomorphic *pax6* genotype had defects in the anterior segment, which included the cornea, lens and iris. The iris in mutant animals, while bilayered, was generally reduced in length and dysmorphic compared to wild-type animals (3 out of 3 hypomorphic mutants examined so far). In the most severely affected mutant examined, iridolenticular and keratolenticular adhesions were apparent (circle in Fig. 12B). For comparison, iris hypoplasia was observed in 90% of the mice examined (Fig. 12D″), and iridokeratotic, iridolenticular and keratolenticular adhesions were observed in about 30% of the same animals ($n=40$). An example of an iridolenticular adhesion is shown in Fig. 12D′ and iridokeratotic

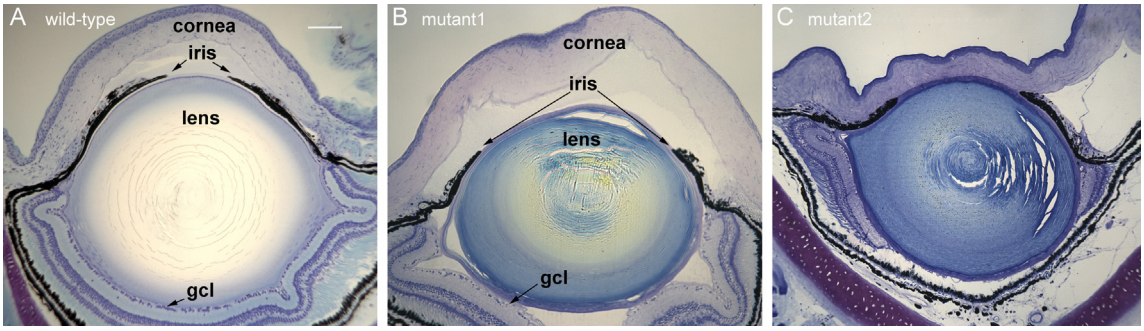

Fig. 11. General histologic features of aniridia-like mutant froglet eyes. Compared with wild-type eyes (A), these mutants show variable defects in cornea, iris, lens and retina. Most notably, the pupil diameter is much wider in the mutants (B and C). Lenses show variable reduction in size and differentiation consistent with the variable presence of cataracts visible upon gross inspection of eyes of intact animals. While the retina is usually present and grossly normal, it may contain folds and the ganglion cell layer (gcl) is somewhat sparse and irregular. The retina may be partially absent as shown in C. Scale bar in panel $A = 100\ \mu m$.

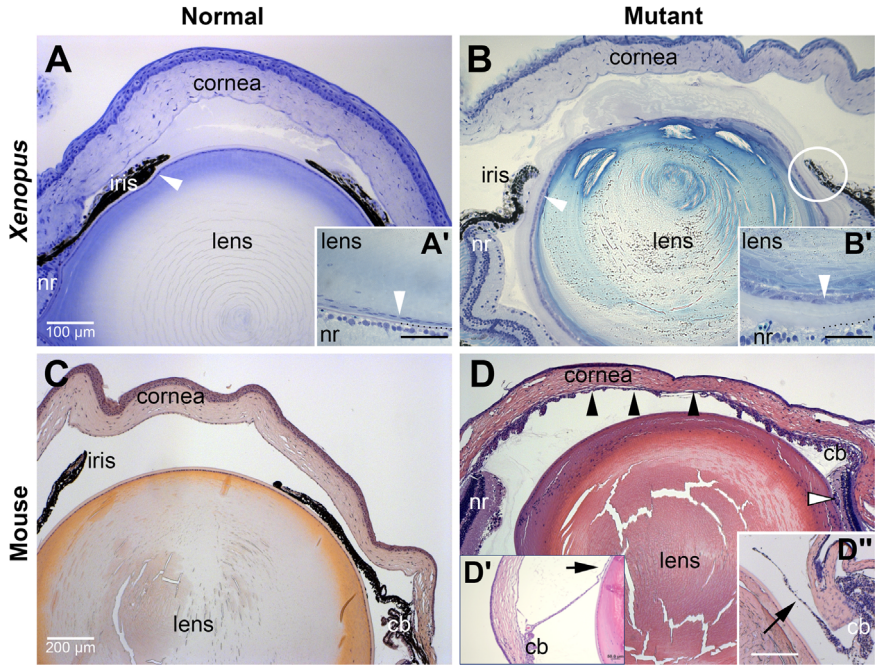

Fig. 12. *Xenopus* mutants for *pax6* exhibit anterior eye defects comparable to those observed in *Pax6* mutant mice. Histological sections cut through eyes from either wild-type (Normal) or *Pax6* mutant (Mutant) *X. tropicalis* (*Xenopus*) and mice (Mouse) showing anterior structures. (A) Wild-type froglet eye. White arrowhead denotes lens epithelial cells. (A′) High magnification view of lens epithelial cells in region of lens adjacent to retina. Dotted line denotes boundary between lens and retina. (B) *pax6* Hypomorphic froglet eye. In addition to the eye being smaller, defects in the cornea, iris, and lens are evident. Circle indicates region with likely iridolenticular adhesion. (B′) High magnification view of lens epithelial cells in region of lens adjacent to retina comparable to A′. Dotted line denotes boundary between lens and retina. Note expansion of acellular material between lens and retina compared to wild-type. (C) 8-Week-old adult wild-type mouse (D) 8-week-old adult $Pax6^{Sey\text{-}Neu/+}$ mouse. Black arrowheads denote iridokeratotic adhesion. Open arrowhead denotes iris or ciliary tissues. (D′) Arrow shows iridolenticular adhesion in section cut from different $Pax6^{Sey\text{-}Neu/+}$ mouse. (D″) Arrow shows iris hypoplasia typically observed in these $Pax6^{Sey\text{-}Neu/+}$ mice; this section was cut from a third $Pax6^{Sey\text{-}Neu/+}$ mouse at a plane comparable to that of the wild-type mouse in C. cb, ciliary body; nr, neuroretina. Scale bar in panel A applies to panel B; scale bar in C applies to panel D. Scale bars in A′, B′ and D′ denote 50 μm. Scale bar in D″ denotes 200 μm.

adhesions are denoted with black arrowheads in Fig. 12D. No iris defects were observed in wild-type littermates (Fig. 12C, $n = 40$). Lens defects were comparable between *pax6* mutant frogs and mutant mice, and included cataracts in 16% of frogs ($n = 12$) and approximately 67% of the mice ($n = 40$). In the hypomorphic *Xenopus* mutants, the lens epithelium was typically more cuboidal than the highly flattened epithelium of wild-type frogs (arrowheads in Fig.12A′ and B′). Larger epithelial cells are occasionally observed in the lenses of more severely affected mutant mice (data not shown).

Most if not all individuals with aniridia will develop a keratopathy known as aniridia-related keratopathy (ARK), which is caused by a breakdown of the corneal epithelium and invasion of conjunctival cells (Holland et al., 2003; Mayer et al., 2003; Netland et al., 2011). To assess the effect of *pax6* mutations in frogs compared to mammals, histological sections of cornea were compared to those from $Pax6^{Sey\text{-}Neu/+}$ mice and the cornea of an individual with aniridia (Fig. 13). The patient was diagnosed with stage III keratopathy and had essentially full conjunctivalization of the cornea (i.e., corneal epithelial cells were largely replaced by cells from the conjunctiva). The sample here was taken from the limbal area as a result of a surgical procedure to repair the cornea.

The cornea of the wild-type frog is structurally similar to that of mouse and human (Fig. 13A, C and E, respectively) and consists of an outer epithelium, stroma and endothelial layer (Fig. 13A). The epithelium, which accounts for approximately 10% of the corneal thickness, consists of a basal layer composed of a single row of cuboidal to short columnar basal cells, followed by 1–2 layers of intermediate (wing) cells and one to two layers of flattened superficial cells. The epithelium is separated from the stroma by

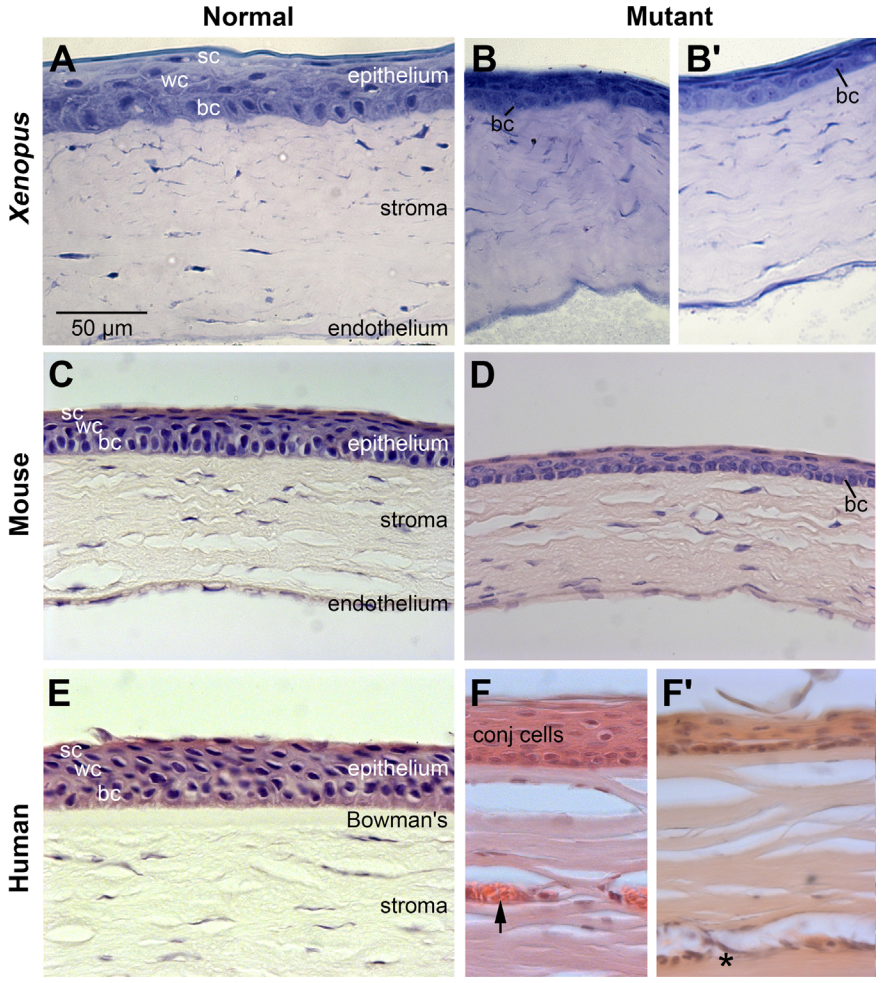

Fig. 13. *Xenopus pax6* mutant exhibits corneal defects similar to those observed in *Pax6* mutant mice and human aniridia. Histology of the cornea of wild-type (Normal) and *Pax6* mutant (Mutant) frog (*Xenopus*), mice (Mouse), and human (Human). (A) Wild-type froglet. (B) *pax6* Hypomorphic froglet. (C) 8-Week-old adult wild-type mouse (D) 8-Week-old adult $Pax6^{Sey\text{-}Neu/+}$ mouse. (E) 70-Year-old human. The cornea did not show clinical signs of keratopathy. (F–F′) 49-Year-old individual with classical aniridia. The patient was diagnosed with stage III keratopathy and exhibited full conjunctivalization of the cornea. Arrow denotes blood vessel. Asterisk denotes area of cellular infiltration in the superficial corneal stroma. The samples here were of peripheral cornea. *Note*: the endothelial layer was not captured in these images of human cornea. bc, basal cells; conj, conjunctival cells, sc, superficial cells; wc, wing cells. Scale bar in panel A applies to panels (B–F). (For interpretation of the references to color in this figure legend, the reader is referred to the web version of this article.)

an acellular (Bowman's) layer, which can be difficult to see by light microscopy. The corneal stroma, which accounts for approximately 90% of the corneal thickness, exhibits a generally well organized, horizontally arranged laminar appearance with flattened spindle-shaped keratocytes, and is avascular. A corneal endothelium, which consists of a single layer of cells, is present on the posterior surface of the cornea.

Histological analysis of the corneas from *pax6* mutant frogs revealed that, similar to mice and humans heterozygous null for *Pax6* (Fig. 13D and F′, respectively), the corneal epithelium of *pax6* hypomorphic frogs appeared to have fewer cell layers and was generally lacking the more differentiated superficial cells compared to the cornea of wild-type frogs (compare Fig. 13B, B′–A). At the histological level, whereas basal cells in the wild-type animals contained round to oval nuclei that stained darkly with toluidine blue, basal cell nuclei in the mutant corneas tended to be lightly stained with a punctate appearance. This staining pattern was also observed in the corneas from *Pax6* mutant mice using hematoxylin (compare Fig. 13D–C). Both touidine blue and hematoxylin stain chromatin. A similar comparison could not be performed on the aniridia cornea because the normal basal cells were largely absent from the samples provided (Fig. 13F, data not shown). Rather the peripheral epithelial layer was composed primarily of cells with a conjunctival like morphology (Fig. 13F); more centrally (Fig. 13F′), the aniridic cornea exhibited a thinned and roughened appearance, consistent with a loss of corneal epithelial cells.

In both frogs and mice mutant for *Pax6*, the anterior stroma typically contained densely packed and disorganized collagenous lamella, which had a wavy appearance, and this was similar to the stroma observed in the cornea from the individual with aniridia (Fig. 13B, B′, D, F and F′). In contrast with the corneas from mutant frogs, goblet cells were present in the epithelium of approximately 80% of $Pax6^{Sey\text{-}Neu/+}$ mice ($n=39$) and in the human aniridia sample. Additionally, blood vessels were observed in the peripheral to mid anterior stroma in all corneal samples from $Pax6^{Sey\text{-}Neu/+}$ mice ($n=39$) and in the human aniridia sample (arrow in Fig. 13F). Areas of cellular infiltration, indicative of inflammatory response, were also observed in the superficial aniridic corneal stroma (asterisk in Fig. 13F′); similar infiltrations were present in the corneal stroma of the more severely affected $Pax6^{Sey\text{-}Neu/+}$ mice (data not shown). Both neovascularization of the cornea and cellular infiltration in the stroma are progressive changes associated with breakdown of corneal epithelium and become more pronounced with age. Children with aniridia and juvenile *Small eye* mice generally have clear corneas without evidence of inappropriate vascularization or evidence of inflammation. Therefore, it is likely that the apparent lack of neovascularization in the corneas of the

froglets is due to their young age rather than a fundamental difference in the progression of keratopathy between frogs, mice, and humans.

Discussion

By utilizing gene editing TALENs technology we have generated an allelic series of mutant lines in the *pax6* gene in *X. tropicalis* that provide a powerful context for studying *pax6* function in development and disease, augmenting in significant new ways what can be accomplished with other model organisms. These lines have already begun to provide valuable new insights about the role of *pax6* gene regulation during development and will continue to be an important source of clearer understanding about *pax6* function during development.

Generation and phenotypic analysis of out-of-frame exon 7 and 9 pax6 mutations

The mutations that we have generated, while targeted to a particular locus, are heterogeneous within this locus because the TALEN technology used here generates different size deletions and inserts within single embryos at different times and in different cell lineages. While this approach creates some complexity in genotyping F0 and F1 animals it also has presented opportunities to identify a variety of alleles that yielded the different phenotype outcomes we discuss here. In the future this methodology should be very valuable in generating other alleles that would permit novel investigations of Pax6 protein activity, dosage and phenotypic effects. We consider here first the group of exon 7 and 9 out-of-frame mutations that lead to a consistent, strong embryonic phenotype and are likely null mutations.

These mutants highlight the utility of the *Xenopus* system for capitalizing on this gene editing technology but generating them requires careful titration of injected constructs. Targeting genes essential for development, like *pax6*, likely implies that one will generate lethal phenotypes if the mutation rate is high. While one can reduce the mutation frequency by reducing TALEN concentrations, at a low hit rate, germline transmission is inefficient and screening of F1 offspring becomes problematic. We find that injecting at relatively high doses, in conjunction with the mosaic nature of the process, provides the advantage that some animals have high mutation rates in only some cells, giving rise to individual animals with a very high germline transmission rate (up to 100% in a few animals we have generated). As described in the Results section, with the *pax6* gene we can often identify animals of this kind because one eye will be severely impacted but not the other. Having animals (particularly males, which can be mated weekly) carrying such a high level of mutations is clearly advantageous in generating a high frequency of F1 mutant embryos for detailed study. This is an especially valuable feature when one considers the long reproductive lifespan of *Xenopus* (we have animals which are 10 years old and still fertile).

The diversity of mutations produced also allowed us to compare phenotypes generated in F1 animals by various mutations. In this paper we show that putative null mutations toward the end of the paired domain in exon 7, predicted to be null based on the target site similarity to mutations in mouse and rat that are thought to be null (discussed earlier), have a characteristic eye phenotype (loss of ventral retina and no lens). Mutations in exon 9 (in the *pax6* homeodomain), and deletions that include the region between exon 7 and 9 all have this characteristic phenotype, suggesting that all of these are likely to be null mutations. In addition these results imply that the unique transcript generated from the α promoter, the paired-less form of *pax6*, Pax6ΔPD, which would be truncated by the exon 9 deletion within the homeodomain but remains intact in exon 7 mutations, does not contribute in a discernable way to early eye development.

As noted in the Introduction, the rationale for proposing that the mouse *Sey* mutation is a null and that typical aniridia mutations in humans are as well (and our mutations in *X. tropicalis pax6*) come from the observation that the phenotypes of the mammalian mutants are indistinguishable from those resulting from deletions spanning the *Pax6* gene. It has also been argued that nonsense mediated decay (NMD), which is known to cause mRNA degradation in response to premature stop codon mutations by a well characterized mechanism (Chang et al., 2007), is responsible for the null phenotype in such *PAX6* mutations (e.g. Vincent et al., 2003). Although it has been shown that NMD machinery exists in *Xenopus*, at least in oocytes (Whitfield et al., 1994), we found that *pax6* transcripts persist in our mutants based on *in situ* hybridization in the tadpole brain (Fig. 7) and at earlier stages as well (data not shown), even though there is a stop codon shortly following the mutation site in the 7th exon responsible for the mutant shown in Fig. 7 as in all exon 7 mutations of this type. Similarly, mutant *Pax6* transcripts are present in mid-gestation mouse embryos homozygous mutant for the Sey^{Neu} allele ($Pax6^{Sey\text{-}Neu/Sey\text{-}Neu}$) at levels comparable to wildtype *Pax6* (Mastick et al., 1997; and Lauderdale, unpublished). In addition, another study on a premature stop codon mutation in *Xenopus*, in this case the eye regulatory gene *rax* (Fish et al., 2014) also shows embryonic expression of the mutant RNA. Within the nervous system there is also evidence that a microRNA, miR-128, inhibits NMD in embryos of several vertebrates, including *Xenopus* (Bruno et al., 2011). We have preliminary evidence (Qiu, Nakayama and Grainger, unpublished) that this microRNA is expressed in the embryonic eye, brain and neural tube. All of this data together with recent reports suggesting that NMD is not a universal phenomenon in stop codon mutations (e.g. Neu-Yilik et al., 2011) argue that NMD is not a primary mechanism for regulating expression of premature stop codon mutants in *pax6* and possibly more broadly in embryogenesis.

If we accept the hypothesis that *pax6* mutations in exon 7 and exon 9 are null, we would invoke the proposal discussed earlier that *pax6.2* plays a role in mitigating the degree of the retinal phenotype in our mutants. We have already used CRISPR-mediated gene targeting to mutate the *pax6.2* and are currently raising animals to evaluate the contribution of this gene to eye development. It has been shown that in zebrafish, an antisense morpholino oligonucleotide directed against *pax6.2* does reduce eye size in wild-type embryos (Ravi et al., 2013). Our analysis of expression of *pax6.2* is consistent with a role in retinal phenotype in the *pax6* mutant because, as noted earlier, expression is restricted to the dorsal retina (which persists in the mutant), but also we note that *pax6.2* is not expressed in the lens, and that the lens is completely absent in the *pax6* mutant. In addition *pax6.2* is not expressed early in development, nor in the brain and the alterations we see in expression of genes like *myc* and *mab21l1* in the early retina (Fig. 6) and brain later (Fig. 7) are consistent with a null phenotype in these domains of *pax6* activity. The significant effect of *pax6.2* on retina formation is somewhat surprising given its late onset of expression.

pax6 Gene targets in putative null mutants

We report here some preliminary findings about expression of putative gene targets of *pax6* that both highlight new observations and the gaps in our understanding of *pax6* regulation of patterning. As noted in the Introduction, there are few studies of the earliest *pax6* targets, likely to be a group of genes that would be highly informative about the primary roles of this gene both in development and disease. In our work we have shown, as in mammals, that the nuclear protein gene *mab21l1* is highly reduced in the eye region in our putative *pax6* null embryos. Gene targeting of *mab21l1* in mice reveals that this gene is essential for lens

formation (Yamada et al., 2003) and a future area of interest will be to ascertain the extent to which the failure of the lens to form in the *pax6* mutant is related to its effect on *mab21l1* expression.

Because the *myc* gene is expressed in a large part of the early *pax6*-expressing domain and is so important in pluripotency and maintaining progenitor cells in a number of developmental contexts (Prasad et al., 2012; Smith and Dalton, 2010), roles which fit within the framework of *pax6* function in pluripotency regulation and neurogenesis (e.g. Sansom et al., 2009), we decided to examine the expression of *myc* at the neural plate stage, shortly after *pax6* activation. Previously, we found *myc* to be downregulated in another key eye gene required for retina specification, *rax* (Fish et al., 2014). As shown in Fig. 6 *myc* is indeed downregulated in the retina, and in the lens ectoderm as well, implying a potentially important role in both of these components of the eye. In other studies, targeted downregulation of the *myc* gene by morpholino antisense oligonucleotide injection into the blastomeres giving rise to the head region in *Xenopus laevis* embryos is shown to interfere with eye development (Bellmeyer et al., 2003). A recent study also highlights the role of *Myc* in cell proliferation during mouse lens development (Cavalheiro et al., 2014). Further studies on the function of *myc* as a potential mediator of *pax6* activity will be an important goal for the future. A more thorough study of putative gene targets by RNA-Seq analysis, as was performed in our *rax* mutant study in *X. tropicalis* (Fish et al., 2014), will be instrumental in elucidating the core genes involved in the eye and neural gene regulatory network involved in the specification events that occur by the neural plate stage (Saha and Grainger, 1992).

Preliminary examinations of expression of putative *pax6* targets in the brain and pancreas are also informative. In the work presented here we see expression of several key brain regulators that have been shown to be *pax6* targets in previous studies and find that they modulate gene expression in ways similar to those seen in mammals, illustrating the requirement for positive feedback to maintain *Pax6* expression in some regions of the diencephalon (Mastick et al., 1997) and substantiating its role in dorsal/ventral patterning in the forebrain (Georgala et al., 2011). However, as discussed above, the role of *pax6* in initial patterning events remains largely unexamined, though *Xenopus* appears to preserve many of the brain functions of *Pax6* in mammals and again should serve as a valuable model for examining these early events. Turning to the activity of *pax6* in the pancreas, again our data on insulin in the *pax6* mutant *Xenopus* indicates the conservation of function in this organ as well, as reported elsewhere (Pearl et al., 2009).

Hypomorphic mutations in pax6 lead to an aniridia-like phenotype

The genetic lesions that do not lead to obvious embryonic phenotypes, but elicit an aniridia-like phenotype in froglets, reveal further important features of the TALEN-mediated mutations in *X. tropicalis*. As background information, we note that animals carrying heterozygous mutations that we believe are null (e.g. frameshift mutations in exon 7) have no obvious eye phenotype, whereas in mammals mutations of this kind would yield an aniridia phenotype. This may suggest a compensatory role of the *pax6.2* gene. In addition it is also possible that the activity of *pax6* itself, or the genetic context in *Xenopus* differs slightly from that in mammals. It is known that in mice eye development is adversely affected by modest changes (either reductions or increases) in the level of Pax6 (Schedl et al., 1996). While raising F1 froglets with complex genotypes we noticed some which developed aniridia and it was at this point that we ascertained that animals carrying one putative null allele and one allele with a small in-frame deletion might be hypomorphs, which are likely to have less than one-half of the wild-type level of Pax6 activity. As noted in the Results section, all of the animals with the hypomorphic phenotype include deletions at or adjacent to amino acid 128, a conserved paired domain residue that causes aniridia in a number of patients as a result of missense mutations and which contacts the major groove of DNA (van Heyningen and Williamson, 2002). These results highlighted to us a previously unappreciated potential value of small in-frame deletions in helping to pinpoint key regions associated with a particular gene function. In the future we intend to identify this kind of lesion in targeted regions of the *pax6* gene outside of the paired domain (where most aniridia-causing mutations are found). As pointed out by others (van Heyningen and Williamson, 2002), while most of the human mutations in *PAX6* that have been identified affect the eye, this finding may be a product of observational bias, as generally only patients presenting with eye-related diseases would be likely to have their *PAX6* locus sequenced. Further identification of vertebrate model phenotypes in other tissues where *pax6* is expressed, and which are caused by *pax6* mutant alleles with lesions in other key regions of the protein, may reveal novel connections to human disease.

Importantly, we show for the first time that mutations in the *Pax6* gene cause similar anterior eye defects in both amphibians and mammals. The structures of the anterior segment of the vertebrate eye, which include the cornea, iris, ciliary body, and lens, are required to focus the light that enters the eye and to regulate intraocular pressure. Developmental defects of these structures can lead to several debilitating eye diseases, including cataracts, corneal dystrophies, and glaucoma. Despite much work in rodent models over the past several decades, a detailed understanding of the molecular mechanisms and genetic hierarchies involved in anterior segment formation is still lacking. Our results demonstrate that, at least in the case of *Pax6*, the mechanisms controlling these processes have been conserved between humans, rodents, and *X. tropicalis*, which last shared a common ancestor approximately 350 million years ago (Hedges and Kumar, 2002), and demonstrate *Xenopus* as an important new vertebrate model for investigations addressing eye problems of significant interest to human health.

Author contributions

T.N., M.F., A.O.O., K.B.Z., M.B.F., J.L.C., and J.D.L. performed experiments. K.N. and Y.Y. designed and constructed TALEN plasmids, and performed preliminary experiments to test activity of TALENs to choose the best target sequences to use. T.N., M.F., A. O.O., J.L.C., J.D.L., P.A.N. and R.M.G. analyzed data. T.N. and R.M.G. conceived the study, and wrote the manuscript with M.F. and J.D.L.

Funding

This work was funded by grants from the National Institutes of Health [NIH R01 EY017400, EY018000 and EY022954] to R.M.G. and research awards from the Sharon Stewart Aniridia Trust to R.M.G. and J.D.L. and also by the Grant-in-Aid for Scientific Research from the Ministry of Education, Culture, Sports, Science and Technology, Japan, [Grant Number 25430089] to K.N. and [Grant Number 26440057] to Y.Y.

Acknowledgements

We thank past and current Grainger lab members for valuable discussions. We also thank Christopher H. K. Cheng and Hui Zhao for sharing pCS2+TALEN-ELD/KKR plasmids, and Daniel F. Voytas

for the Golden Gate TALEN and the TAL effector kit (Addgene, #1000000016). We appreciate consultations with Veronica van Heyningen and Noriko Osumi regarding information about mouse and rat *Pax6* mutations, and Ira Blitz for pointing out the possibility of the presence of a second *pax6* gene (*pax6.2*) locus found while annotating the *X. tropicalis* genome. We also gratefully acknowledge Sharon Levasseur for her participation in the clinical evaluation of the aniridic phenotype in *X. tropicalis* mutants. In addition we would like to thank John Freeman for providing human tissue used in these studies. Finally, the authors gratefully acknowledge support of the National *Xenopus* Resource and its staff, from which *pax6* mutant frogs described here will be available.

Appendix A. Supporting information

Supplementary data associated with this article can be found in the online version at http://dx.doi.org/10.1016/j.ydbio.2015.02.012.

References

Bellmeyer, A., Krase, J., Lindgren, J., LaBonne, C., 2003. The protooncogene c-Myc is an essential regulator of neural crest formation in *Xenopus*. Dev. Cell 4, 827–839.

Bernier, G., Vukovich, W., Neidhardt, L., Herrmann, B.G., Gruss, P., 2001. Isolation and characterization of a downstream target of *Pax6* in the mammalian retinal primordium. Development 128, 3987–3994.

Blitz, I.L., Biesinger, J., Xie, X., Cho, K.W.Y., 2013. Biallelic genome modification in F_0 *Xenopus tropicalis* embryos using the CRISPR/Cas system. Genesis 51, 827–834.

Bruno, I.G., Karam, R., Huang, L., Bhardwaj, A., Lou, C.H., Shum, E.Y., Song, H.-W., Corbett, M.A., Gifford, W.D., Gecz, J., Pfaff, S.L., Wilkinson, M.F., 2011. Identification of a microRNA that activates gene expression by repressing nonsense-mediated RNA decay. Mol. Cell 42, 500–510.

Callaerts, P., Halder, G., Gehring, W.J., 1997. *PAX-6* in development and evolution. Annu. Rev. Neurosci. 20, 483–532.

Carney, R.S.E., Cocas, L.A., Hirata, T., Mansfield, K., Corbin, J.G., 2009. Differential regulation of telencephalic pallial–subpallial boundary patterning by *Pax6* and *Gsh2*. Cerebral Cortex 19, 745–759.

Cavalheiro, G.R., Matos-Rodrigues, G.E., Gomes, A.L., Rodrigues, P.M.G., Martins, R.A. P., 2014. c-myc regulates cell proliferation during lens development. PLoS One 9, e87182.

Cermak, T., Doyle, E.L., Christian, M., Wang, L., Zhang, Y., Schmidt, C., Baller, J.A., Somia, N.V., Bogdanove, A.J., Voytas, D.F., 2011. Efficient design and assembly of custom TALEN and other TAL effector-based constructs for DNA targeting. Nucleic Acids Res. 39, e82.

Chang, Y.-F., Imam, J.S., Wilkinson, M.F., 2007. The nonsense-mediated decay RNA surveillance pathway. Annu. Rev. Biochem. 76, 51–74.

Coutinho, P., Pavlou, S., Bhatia, S., Chalmers, K.J., Kleinjan, D.A., van Heyningen, V., 2011. Discovery and assessment of conserved Pax6 target genes and enhancers. Genome Res. 21, 1349–1359.

Engelkamp, D., Rashbass, P., Seawright, A., van Heyningen, V., 1999. Role of *Pax6* in development of the cerebellar system. Development 126, 3585–3596.

Favor, J., Gloeckner, C.J., Neuhäuser-Klaus, A., Pretsch, W., Sandulache, R., Saule, S., Zaus, I., 2008. Relationship of *Pax6* activity levels to the extent of eye development in the mouse, *Mus musculus*. Genetics 179, 1345–1355.

Favor, J., Peters, H., Hermann, T., Schmahl, W., Chatterjee, B., Neuhäuser-Klaus, A., Sandulache, R., 2001. Molecular characterization of $Pax6^{2Neu}$ through $Pax6^{10Neu}$: an extension of the *Pax6* allelic series and the identification of two possible hypomorph alleles in the mouse *Mus musculus*. Genetics 159, 1689–1700.

Fish, M.B., Nakayama, T., Fisher, M., Hirsch, N., Cox, A., Reeder, R., Carruthers, S., Hall, A., Stemple, D.L., Grainger, R.M., 2014. *Xenopus* mutant reveals necessity of *rax* for specifying the eye field which otherwise forms tissue with telencephalic and diencephalic character. Dev. Biol. 395, 317–330.

Fish, M.B., Nakayama, T., Grainger, R.M., 2012. Simple, fast, tissue-specific bacterial artificial chromosome transgenesis in *Xenopus*. Genesis 50, 307–315.

Gehring, W.J., Ikeo, K., 1999. *Pax 6*: mastering eye morphogenesis and eye evolution. Trends Genet. 15, 371–377.

Georgala, P.A., Carr, C.B., Price, D.J., 2011. The role of Pax6 in forebrain development. Dev. Neurobiol. 71, 690–709.

Glaser, T., Jepeal, L., Edwards, J.G., Young, S.R., Favor, J., Maas, R.L., 1994. *PAX6* gene dosage effect in a family with congenital cataracts, aniridia, anophthalmia and central nervous system defects. Nat. Genet. 7, 463–471.

González, A., López, J.M., Marín, O., 2002. Expression pattern of the homeobox proteinNKX2-1 in the developing *Xenopus* forebrain. Gene Expr. Patterns 1, 181–185.

Guo, X., Zhang, T., Hu, Z., Zhang, Y., Shi, Z., Wang, Q., Cui, Y., Wang, F., Zhao, H., Chen, Y., 2014. Efficient RNA/Cas9-mediated genome editing in *Xenopus tropicalis*. Development 141, 707–714.

Harland, R.M., Grainger, R.M., 2011. *Xenopus* research: metamorphosed by genetics and genomics. Trends Genet. 27, 507–515.

Hedges, S.B., Kumar, S., 2002. Genomics. Vertebrate genomes compared. Science 297, 1283–1285.

Hellsten, U., Harland, R.M., Gilchrist, M.J., Hendrix, D., Jurka, J., Kapitonov, V., Ovcharenko, I., Putnam, N.H., Shu, S., Taher, L., Blitz, I.L., Blumberg, B., Dichmann, D.S., Dubchak, I., Amaya, E., Detter, J.C., Fletcher, R., Gerhard, D.S., Goodstein, D., Graves, T., Grigoriev, I. V., Grimwood, J., Kawashima, T., Lindquist, E., Lucas, S.M., Mead, P.E., Mitros, T., Ogino, H., Ohta, Y., Poliakov, A.V., Pollet, N., Robert, J., Salamov, A., Sater, A.K., Schmutz, J., Terry, A., Vize, P.D., Warren, W.C., Wells, D., Wills, A., Wilson, R.K., Zimmerman, L.B., Zorn, A.M., Grainger, R., Grammer, T., Khokha, M.K., Richardson, P. M., Rokhsar, D.S., 2010. The genome of the Western clawed frog *Xenopus tropicalis*. Science 328, 633–636.

Hill, M.E., Asa, S.L., Drucker, D.J., 1999. Essential requirement for *Pax6* in control of enteroendocrine proglucagon gene transcription. Mol. Endocrinol. 13, 1474–1486.

Hill, R.E., Favor, J., Hogan, B.L.M., Ton, C.C.T., Saunders, G.F., Hanson, I.M., Prosser, J., Jordan, T., Hastie, N.D., van Heyningen, V., 1991. Mouse *Small eye* results from mutations in a paired-like homeobox-containing gene. Nature 354, 522–525.

Hingorani, M., Hanson, I., van Heyningen, V., 2012. Aniridia. Eur. J. Human Genet. 20, 1011–1017.

Hirsch, N., Harris, W.A., 1997. *Xenopus* Pax-6 and retinal development. J. Neurobiol. 32, 45–61.

Hirsch, N., Zimmerman, L.B., Gray, J., Chae, J., Curran, K.L., Fisher, M., Ogino, H., Grainger, R.M., 2002. *Xenopus tropicalis* transgenic lines and their use in the study of embryonic induction. Dev. Dyn. 225, 522–535.

Hogan, B.L.M., Hirst, E.M.A., Horsburgh, G., Hetherington, C.M., 1988. *Small eye (Sey)*: a mouse model for the genetic analysis of craniofacial abnormalities. Development 103 (Suppl.), 115–119.

Hogan, B.L.M., Horsburgh, G., Cohen, J., Hetherington, C.M., Fisher, G., Lyon, M.F., 1986. *Small eyes (Sey)*: a homozygous lethal mutation on chromosome 2 which affects the differentiation of both lens and nasal placodes in the mouse. J. Embryol. Exp. Morphol. 97, 95–110.

Holland, E.J., Djalilian, A.R., Schwartz, G.S., 2003. Management of aniridic keratopathy with keratolimbal allograft: a limbal stem cell transplantation technique. Ophthalmology 110, 125–130.

Holm, P.C., Mader, M.T., Haubst, N., Wizenmann, A., Sigvardsson, M., Götz, M., 2007. Loss- and gain-of-function analyses reveal targets of Pax6 in the developing mouse telencephalon. Mol. Cell. Neurosci. 34, 99–119.

Illes, J.C., Winterbottom, E., Isaacs, H.V., 2009. Cloning and expression analysis of the anterior parahox genes, *Gsh1* and *Gsh2* from *Xenopus tropicalis*. Dev. Dyn. 238, 194–203.

Ishibashi, S., Cliffe, R., Amaya, E., 2012. Highly efficient bi-allelic mutation rates using TALENs in *Xenopus tropicalis*. Biol. Open 1, 1273–1276.

Kim, J., Lauderdale, J.D., 2006. Analysis of Pax6 expression using a BAC transgene reveals the presence of a paired-less isoform of Pax6 in the eye and olfactory bulb. Dev. Biol. 292, 486–505.

Kim, J., Lauderdale, J.D., 2008. Overexpression of pairedless Pax6 in the retina disrupts corneal development and affects lens cell survival. Dev. Biol. 313, 434–454.

Kokotas, H., Petersen, M.B., 2010. Clinical and molecular aspects of aniridia. Clin. Genet. 77, 409–420.

Lei, Y., Guo, X., Liu, Y., Cao, Y., Deng, Y., Chen, X., Cheng, C.H., Dawid, I.B., Chen, Y., Zhao, H., 2012. Efficient targeted gene disruption in *Xenopus* embryos using engineered transcription activator-like effector nucleases (TALENs). Proc. Natl. Acad. Sci. U.S.A. 109, 17484–17489.

Manuel, M., Price, D.J., 2005. Role of Pax6 in forebrain regionalization. Brain Res. Bull. 66, 387–393.

Mastick, G.S., Davis, N.M., Andrew, G.L., Easter Jr., S.S., 1997. *Pax-6* functions in boundary formation and axon guidance in the embryonic mouse forebrain. Development 124, 1985–1997.

Matsuo, T., Osumi-Yamashita, N., Noji, S., Ohuchi, H., Koyama, E., Myokai, F., Matsuo, N., Taniguchi, S., Doi, H., Iseki, S., et al., 1993. A mutation in the Pax-6 gene in rat *small eye* is associated with impaired migration of midbrain crest cells. Nat. Genet. 3, 299–304.

Mayer, K.L., Nordlund, M.L., Schwartz, G.S., Holland, E.J., 2003. Keratopathy in congenital aniridia. Ocul. Surf. 1, 74–79.

Moreno, N., Rétaux, S., González, A., 2008. Spatio-temporal expression of *Pax6* in *Xenopus* forebrain. Brain Res. 1239, 92–99.

Nakajima, K., Nakai, Y., Okada, M., Yaoita, Y., 2013. Targeted gene disruption in the *Xenopus tropicalis* genome using designed TALE nucleases. Zool. Sci. 30, 455–460.

Nakajima, K., Yaoita, Y., 2013. Comparison of TALEN scaffolds in *Xenopus tropicalis*. Biol. Open 2, 1364–1370.

Nakayama, T., Fish, M.B., Fisher, M., Oomen-Hajagos, J., Thomsen, G.H., Grainger, R.M., 2013. Simple and efficient CRISPR/Cas9-mediated targeted mutagenesis in *Xenopus tropicalis*. Genesis 51, 835–843.

Netland, P.A., Scott, M.L., Boyle IV, J.W., Lauderdale, J.D., 2011. Ocular and systemic findings in a survey of aniridia subjects. J. AAPOS 15, 562–566.

Neu-Yilik, G., Amthor, B., Gehring, N.H., Bahri, S., Paidassi, H., Hentze, M.W., Kulozik, A.E., 2011. Mechanism of escape from nonsense-mediated mRNA decay of human ß-globin transcripts with nonsense mutations in the first exon. RNA 17, 843–854.

Nieuwkoop, P.D., Faber, J., 1994. Normal Table of *Xenopus laevis*. Garland Publishing Inc., New York.

Numayama-Tsuruta, K., Arai, Y., Osumi, N., 2007. The rat *Small eye* homozygote ($rSey^2/rSey^2$) can be regarded as a *Pax6* null mutant. In: Esashi, M., Ishii, K.,

Ohuchi, N., Osumi, N., Sato, M., Yamaguchi, T. (Eds.), Future Medical Engineering Based on Bionanotechnology: Proceedings of the Final Symposium of the Tohoku University 21st Century Center for Excellence Program. Imperial College Press, pp. 151-161.

Ogino, H., McConnell, W.B., Grainger, R.M., 2006. High-throughput transgenesis in *Xenopus* using *I-SceI* meganuclease. Nat. Protoc. 1, 1703–1710.

Osumi, N., Hirota, A., Ohuchi, H., Nakafuku, M., Iimura, T., Kuratani, S., Fujiwara, M., Noji, S., Eto, K., 1997. *Pax-6* is involved in the specification of hindbrain motor neuron subtype. Development 124, 2961–2972.

Osumi, N., Shinohara, H., Numayama-Tsuruta, K., Maekawa, M., 2008. Concise review: Pax6 transcription factor contributes to both embryonic and adult neurogenesis as a multifunctional regulator. Stem Cells 26, 1663–1672.

Pearl, E.J., Bilogan, C.K., Mukhi, S., Brown, D.D., Horb, M.E., 2009. *Xenopus* pancreas development. Dev. Dyn. 238, 1271–1286.

Peng, Y., Clark, K.J., Campbell, J.M., Panetta, M.R., Guo, Y., Ekker, S.C., 2014. Making designer mutants in model organisms. Development 141, 4042–4054.

Prasad, M.S., Sauka-Spengler, T., LaBonne, C., 2012. Induction of the neural crest state: control of stem cell attributes by gene regulatory, post-transcriptional and epigenetic interactions. Dev. Biol. 366, 10–21.

Prosser, J., van Heyningen, V., 1998. *PAX6* mutations reviewed. Hum. Mutat. 11, 93–108.

Ravi, V., Bhatia, S., Gautier, P., Loosli, F., Tay, B.-H., Tay, A., Murdoch, E., Coutinho, P., van Heyningen, V., Brenner, S., Venkatesh, B., Kleinjan, D.A., 2013. Sequencing of *Pax6* loci from the elephant shark reveals a family of *Pax6* genes in vertebrate genomes, forged by ancient duplications and divergences. PLoS Genet. 9, e1003177.

Rice, P., Longden, I., Bleasby, A., 2000. EMBOSS: the European molecular biology open software suite. Trends Genet. 16, 276–277.

Roberts, R.C., 1967. Small eyes—a new dominant mutation in the mouse. Genet. Res. Camb. 9, 121–122.

Saha, M.S., Grainger, R.M., 1992. A labile period in the determination of the anterior–posterior axis during early neural development in Xenopus. Neuron 8, 1003–1014.

Sander, M., Neubüser, A., Kalamaras, J., Ee, H.C., Martin, G.R., German, M.S., 1997. Genetic analysis reveals that PAX6 is required for normal transcription of pancreatic hormone genes and islet development. Genes Dev. 11, 1662–1673.

Sansom, S.N., Griffiths, D.S., Faedo, A., Kleinjan, D.-J., Ruan, Y., Smith, J., van Heyningen, V., Rubenstein, J.L., Livesey, F.J., 2009. The level of the transcription factor Pax6 is essential for controlling the balance between neural stem cell self-renewal and neurogenesis. PLoS Genet. 5, e1000511.

Scardigli, R., Bäumer, N., Gruss, P., Guillemot, F., Le Roux, I., 2003. Direct and concentration-dependent regulation of the proneural gene *Neurogenin2* by Pax6. Development 130, 3269–3281.

Schedl, A., Ross, A., Lee, M., Engelkamp, D., Rashbass, P., van Heyningen, V., Hastie, N.D., 1996. Influence of *PAX6* gene dosage on development: overexpression causes severe eye abnormalities. Cell 86, 71–82.

Shaham, O., Menuchin, Y., Farhy, C., Ashery-Padan, R., 2012. Pax6: a multi-level regulator of ocular development. Prog. Retinal Eye Res. 31, 351–376.

Sive, H.L., Grainger, R.M., Harland, R.M., 2000. Early Development of Xenopus laevis: A Laboratory Manual. Cold Spring Harbor Laboratory Press, New York.

Smith, K., Dalton, S., 2010. *Myc* transcription factors: key regulators behind establishment and maintenance of pluripotency. Regen. Med. 5, 947–959.

St-Onge, L., Sosa-Pineda, B., Chowdhury, K., Mansouri, A., Gruss, P., 1997. *Pax6* is required for differentiation of glucagon-producing α-cells in mouse pancreas. Nature 387, 406–409.

Stoykova, A., Fritsch, R., Walther, C., Gruss, P., 1996. Forebrain patterning defects in *Small eye* mutant mice. Development 122, 3453–3465.

Stoykova, A., Treichel, D., Hallonet, M., Gruss, P., 2000. *Pax6* modulates the dorsoventral patterning of the mammalian telencephalon. J. Neurosci. 20, 8042–8050.

Sturtevant, A.H., 1951. A map of the fourth chromosome of *Drosophila melanogaster*, based on crossing over in triploid females. Proc. Natl. Acad. Sci. U.S.A. 37, 405–407.

Sussel, L., Marin, O., Kimura, S., Rubenstein, J.L.R., 1999. Loss of *Nkx2.1* homeobox gene function results in a ventral to dorsal molecular respecification within the basal telencephalon: evidence for a transformation of the pallidum into the striatum. Development 126, 3359–3370.

Suzuki, K.T., Isoyama, Y., Kashiwagi, K., Sakuma, T., Ochiai, H., Sakamoto, N., Furuno, N., Kashiwagi, A., Yamamoto, T., 2013. High efficiency TALENs enable F0 functional analysis by targeted gene disruption in *Xenopus laevis* embryos. Biol. Open 2, 448–452.

Theiler, K., Varnum, D.S., Stevens, L.C., 1978. Development of Dickie's *Small eye*, a mutation in the house mouse. Anat. Embryol. 155, 81–86.

Toresson, H., Potter, S.S., Campbell, K., 2000. Genetic control of dorsal–ventral identity in the telencephalon: opposing roles for *Pax6* and *Gsh2*. Development 127, 4361–4371.

van Heyningen, V., Williamson, K.A., 2002. *PAX6* in sensory development. Hum. Mol. Gen. 11, 1161–1167.

Vincent, M.-C., Pujo, A.-L., Olivier, D., Calvas, P., 2003. Screening for *PAX6* gene mutations is consistent with haploinsufficiency as the main mechanism leading to various ocular defects. Eur. J. Human Genet. 11, 163–169.

Walther, C., Gruss, P., 1991. *Pax-6*, a murine paired box gene, is expressed in the developing CNS. Development 113, 1435–1449.

Wawersik, S., Purcell, P., Rauchman, M., Dudley, A.T., Robertson, E.J., Maas, R., 1999. BMP7 acts in murine lens placode development. Dev. Biol. 207, 176–188.

Whitfield, T.T., Sharpe, C.R., Wylie, C.C., 1994. Nonsense-mediated mRNA decay in *Xenopus* oocytes and embryos. Dev. Biol. 165, 731–734.

Wolf, L.V., Yang, Y., Wang, J., Xie, Q., Braunger, B., Tamm, E.R., Zavadil, J., Cvekl, A., 2009. Identification of Pax6-dependent gene regulatory networks in the mouse lens. PLoS One 4, e4159.

Yamada, R., Mizutani-Koseki, Y., Hasegawa, T., Osumi, N., Koseki, H., Takahashi, N., 2003. Cell-autonomous involvement of *Mab21l1* is essential for lens placode development. Development 130, 1759–1770.

Yun, K., Potter, S., Rubenstein, J.L., 2001. *Gsh2* and *Pax6* play complementary roles in dorsoventral patterning of the mammalian telencephalon. Development 128, 193–205.